The 15th Symposium on Polar Science

3－5 December 2024

National Institute of Polar Research

Research Organization of Information and Systems

Session OG

Polar Geosciences

Abstracts

Conveners: Kenji Horie, and Yusuke Suganuma (NIPR)

OGo1

Zircon U-Pb dating of ultrahigh-temperature metamorphic rock in Balchenfjella, Sør Rondane Mountains, East Antarctica

Fumiko Higashino[1], Tetsuo Kawakami[1], Shumpei Kudo[1], Miku Nakano[1], Cheolwoo Kim[1], Sota Niki[2] and Takafumi Hirata[3]
[1]*Kyoto University,* [2]*Nagoya University,* [3]*The University of Tokyo*

Ultrahigh-temperature (UHT) metamorphism is regarded as thermally extreme type of crustal metamorphism with temperatures over 900 °C at pressures of 0.5-1.8 GPa (Harley, 2021). The age distribution of UHT metamorphic rocks shows a temporal relationship to supercontinent assembly (Brown, 2006, 2007; Kelsey and Hand, 2015). Using UHT metamorphic rocks as evidence of thermally extreme crustal conditions, they enable us to reveal the tectonothermal mechanism during the orogenesis.

There are controversial arguments that the Sør Rondane Mountains (SRM), East Antarctica are located at almost crossing point of the East African Orogen and the Kuunga Orogen or located within the East African-Antarctic Orogen without the Kuunga Orogeny (Jacobs et al., 2003; Meert, 2003). UHT metamorphic rocks during the Gondwana period are not found in Africa so far, and they are concentrated along the Kuunga Orogen (Harley, 2021). The SRM are located in the middle between Schirmacher Hills and Lützow-Holm Complex, respectively where UHT metamorphism is detected at ca. 650 Ma and ca. 550 Ma (Baba et al., 2010; Durgalakshmi et al., 2021). The first report of UHT metamorphic rock from outcrop in the SRM is a pelitic gneiss from Balchenfjella, eastern SRM (Higashino ant Kawakami, 2022). This supports the previous implication of Grantham et al. (2013) suggesting an initial *P-T* conditions of >900 °C, >1.2 GPa by combining descriptions in Osanai et al. (1996), Asami et al. (1992) and Nakano et al. (2011). Grantham et al. (2013) supports the presence of the Kuunga Orogeny because of multiple zircon U-Pb ages from Balchenfjella, although the *P-T-t* path was not proposed. In this study, therefore, we performed LA-ICPMS zircon U-Pb dating and rare earth analysis of zircon and garnet and discuss the timing of UHT metamorphism in the SRM.

The studied sample is a sillimanite-garnet-biotite gneiss collected from Balchenfjella. UHT metamorphic condition is constrained by ternary feldspar thermometry applied to mesoperthite present in the matrix and included in garnet (Higashino and Kawakami, 2022). Since garnet does not show clear zoning pattern even in phosphorus which diffuses slowly in garnet, it is difficult to define core/rim boundary. HREE concentrations in garnet grains tend to decrease from the geometric center to the margin. Zircon grains are included in garnet, included in mesoperthite in the matrix and also present in the matrix. They are commonly rounded- to oval-shaped and ~100 μm in diameter, showing CL-dark core, CL-bright mantle and CL-dark rim. Zircon included in garnet lacks CL-dark rim. CL-dark core tends to give concordant ^{206}Pb/^{238}U dates of >600 Ma (95-105 % concordance). CL-bright mantle and CL-dark rim also give concordant ^{206}Pb/^{238}U dates of ca. 600-570 Ma (n = 4) and ca. 540-520 Ma (n = 2), respectively. Since core and mantle of zircon included in mesoperthite gave the average concordant ^{206}Pb/^{238}U date of ca. 595 Ma (n = 2), UHT metamorphic condition possibly occurred after ca. 595 Ma.

Array plot of Taylor et al. (2017) is investigated in order to evaluate equilibrium relationship between zircon and garnet. Zircon included in perthite and mesoperthite with Ybn/Gdn ≈ 1.0 is paired with garnet. Pair of zircon and margin of garnet including sillimanite is plotted around the equilibrium point at >900 °C on the array plot, although that of zircon and garnet not including sillimanite is plotted away from the array at >900 °C. This suggests that garnet margin, sillimanite and zircon were in equilibrium with each other under UHT condition. On the other hand, high Ybn/Gdn value of zircon core implies that it was not in equilibrium with garnet.

Timing of UHT metamorphism in the SRM might suggest long-lived regional metamorphism from the East African Orogeny to the Kuunga Orogeny in the deep crust. This is supported by high-temperature duration of ca. 0.5-40 Myr from Balchenfjella (Higashino et al., 2019). Eastward younging of UHT metamorphism along the Dronning Maud Land might imply gradual collision process between northern and southern terranes. Spatial distribution of pressure-temperature-time path should be further examined.

References

Asami, M., Y. Osanai, K. Shiraishi, and H. Makimoto, Metamorphic evolution of the Sør Rondane Mountains, East Antarctica. In Recent Progress in Antarctic Earth Science (Yoshida, Y., Kaminuma, K. and Shiraishi, K. Eds.). Terra Scientific Publishing Company, Tokyo, 7–15, 1992.

Baba, S., T. Hokada, H. Kaiden, D.J. Dunkley, M. Owada, and K. Shiraishi, SHRIMP zircon U-Pb dating of sapphirine-bearing granulite and biotite-hornblende gneiss in the Schirmacher Hills, east Antarctica: implications for Neoproterozoic ultrahigh-temperature metamorphism predating the assembly of Gondwana. The Journal of Geology, 118, 621-639, 2010.

Brown, M., Duality of thermal regimes is the distinctive characteristics of plate tectonics since the Neoarchean. Geology, 34, 961–964, 2006.

Brown, M., Metamorphism, plate tectonics, and the supercontinent cycle. Earth Science Frontiers, 14, 1–18, 2007.

Durgalakshmi, K. Sajeev, I.M. Williams, D.H. Reddy, M. Satish-Kumar, N. Jöns, S.P.K. Malaviarachchi, V.O. Samuel and P.M. George, The timing, duration and conditions of UHT metamorphism in remnants of the former eastern Gondwana. Journal of Petrology, 62, egab068, 2021.

Grantham, G. H., P.H. Macey, K. Horie, T. Kawakami, M. Ishikawa, M. Satish-Kumar, N. Tsuchiya, P. Graser, and S. Azevedo, Comparison of the metamorphic history of the Monapo Complex, northern Mozambique and Balchenfjella and Austhameren areas, Sør Rondane, Antarctica: Implications for the Kuunga Orogeny and the amalgamation of N and S. Gondwana. Precambrian Research, 234, 85-135, 2013.

Harley, S.L., UHT metamorphism. In: Encyclopedia of Geology (Alderton, D. and Elias, S.A. Eds.). Elsevier, 522–552, 2021.

Higashino, F. and T. Kawakami, Ultrahigh–temperature metamorphism and melt inclusions from the Sør Rondane Mountains, East Antarctica. Journal of Mineralogical and Petrological Sciences, 117, 010, 2022.

Higashino, F., D. Rubatto, T. Kawakami, A.S. Bouvier, and L.P. Baumgartner, Oxygen isotope speedometry in granulite facies garnet recording fluid/melt–rock interaction (Sør Rondane Mountains, East Antarctica). Journal of Metamorphic Geology, 37, 1037-1048, 2019.

Jacobs, J., W. Bauer, C.M. Fanning, Late Neoproterozoic/Early Paleozoic events in central Doronning Maud Land and significance for the southern extension of the East African Orogen into East Antarctica. Precambrian Research 126, 27-53, 2003.

Kelsey, D.E. and M. Hand, On ultrahigh temperature crustal metamorphism: Phase equilibria, trace element thermometry, bulk composition, heat sources, timescales and tectonic settings. Geoscience Frontiers, 6, 311–356, 2015.

Meert, J., A synopsis of events related to the assembly of eastern Gondwana. Tectonophysics 362, 1-40, 2003.

Nakano, N., Y. Osanai, S. Baba, T. Adachi, T. Hokada, and T. Toyoshima, Inferred ultrahigh–temperature metamorphism of amphibolitized olivine granulite from the Sør Rondane Mountains, East Antarctica. Polar Science, 5, 345–359, 2011.

Osanai, Y., L. Shiraishi, Y. Takahashi, H. Ishizuka, Y. Moriwaki, N. Tsuchiya, T. Sakiyama, T. Toyoshima, M. Owada, and H. Kojima, Explanatory Text of Geological Map of Brattnipene, Sør Rondane Mountains, Antarctica. National Institute of Polar Research, Tokyo, Japan. 1996.

Taylor, R.J.M., C. Clark, S.L. Harley, A.R.C. Kylander-Clark, B.R. Hacker, and P.D. Kinny, Interpreting granulite facies events through rare earth element partitioning arrays. Journal of Metamorphic Geology, 35, 759-775, 2017.

OGo2

The pressure–temperature conditions of garnet–orthopyroxene granulite from Oku-iwa Rock in the Lützow-Holm Complex, East Antarctica

Ippei Kitano[1], Tsuyoshi Toyoshima[2], Masahiro Ishikawa[3] and Takuma Katori[4]

[1] *The Hokkaido University Museum*

[2] *Niigata University*

[3] *Yokohama National University*

[4] *Fossa Magna Museum*

The Lützow-Holm Complex (LHC), East Antarctica, is composed of high-grade metamorphic rocks and intrusive rocks (e.g., Hiroi et al., 1983). These metamorphic rocks indicate the southwestward increase in metamorphic grade from amphibolite- to granulite-facies with clockwise pressure (*P*)–temperature (*T*) paths and high- to ultrahigh-temperature metamorphic conditions during >600–500 Ma (e.g., Hiroi et al., 1983; Shiraishi et al., 1994). Recent petrological and geochronological studies revealed the LHC is a collage of several terranes with a complicated metamorphic history and required the re-examination throughout the LHC (e.g., Suzuki & Kawakami, 2019; Dunkley et al., 2020; Kitano et al., 2023). Oku-iwa Rock is located in the transitional zone between amphibolite-facies zone in the northeast and granulite-facies zone in the southwest (Hiroi et al, 1983) and is quite limited in petrological studies. Kitano et al. (2020) initially reported the occurrence and petrographical feature of a garnet–orthopyroxene granulite from its central part. Its metamorphic evolution is still unknown but will be key information to understand the thermal history in Oku-iwa Rock. Thus, this study will present the *P*–*T* conditions estimated from the garnet–orthopyroxene granulite with associated rock and vein.

Oku-iwa Rock consists of hornblende–biotite gneiss, migmatitic biotite–hornblende gneiss and leucocratic biotite gneiss wihich are variously migmatized and folded and intruded by granitoid with a Rb–Sr isochhron age of 480 ± 50 Ma (Nakai et al., 1981; Nishi et al., 2002). The garnet–orthopyroxene granulite occurs as a lenticular block with following the foliation of host migmatitic felsic gneiss (Kitano et al., 2020). The anhedral garnet porphyroblast associated with symplectite can be observed only at the center of the block locally associated with leucocratic veins. Toward the margin, garnet and orthopyroxene are completely replaced by biotite + plagioclase symplectite and/or orthoamphibole, respectively. The margin of the block is just composed of foliated amphibolite without symplectite. This study analyzed the granulite with leucocratic vein (IK19011404A) and foliated amphibolite (IK19011404C) collected from the central and marginal parts of the mafic block, resprectively.

The granulite (IK19011404A) has a granoblastic texture and a mineral assemblage of garnet, hornblende, biotite, and plagioclase with minor orthopyroxene, spinel, staurolite, chlorite, quartz, rutile, ilmenite, apatite, magnetite and zircon. Staurolite, spinel, chlorite, quartz, rutile and ilmenite are included in the garnet. Gedrite (to sodic gedrite), anthophyllite, some of spinel, hornblende, biotite, and plagioclase are secondary phases replacing garnet or orthopyroxene. Beside a leucocratic vein, hornblende is partly replaced by cummingtonite. The vein is weakly deformed and composed of hornblende partly replaced by cummingtonite, plagioclase and quartz. The foliated amphibolite (IK19011404C) mainly consists of oriented hornblende, biotite, plagioclase and quartz.

Anhedral garnet porphyroblast in the granulite (IK19011404A) shows a compositional zoning with decrease of Ca, Fe and Mn and increase of Mg toward the margin and the enrichment of Mn and depletion of Mg at the margin. Inclusions of staurolite (X_{Mg} = 0.33−0.36, X_{Zn} = 0.01−0.02), spinel (not on the surface), chlorite (X_{Mg} = 0.66−0.70), quartz, rutile and ilmenite occur in the high-Ca, -Fe, and -Mn, and low-Mg domain of garnet. Its margin is decomposed into the euhedral to subhedral biotite (X_{Mg} = 0.76−0.82) + plagioclase (X_{An} = 0.39−0.59) ± spinel (X_{Mg} = 0.38−0.51, X_{Zn} = 0.04−0.08) ± magnetite ± gedrite symplectite. Anhedral orothopyroxene in the matrix is replaced by either biotite + plagioclase association or anthophyllite and shows small chemical variation of X_{Mg} = 0.67−0.69 and X_{Al} = 0.06−0.09. Biotite included in orthopyroxene and in the matrix has lower X_{Mg} values of 0.76 and 0.74−0.76, respectively. Anorthite contents of plagioclase in magnetite ± ilmenite and in the matrix are 0.42−0.51 and 0.35−0.42, respectively. Spinel in magnetite ± ilmenite shows similar compoisitions (X_{Mg} = 0.38−0.49, X_{Zn} = 0.04−0.08) with those replacing garnet. Hornblende is pargasitic to slightly edenitic and has X_{Mg} values of 0.65−0.66. Anthophyllite replacing orthopyroxene shows higher X_{Mg} (0.70−0.73) than that of gedrite overgrowing anthophyllite and replacing biotite around garnet (X_{Mg} = 0.65−0.69). In the vein intruding into the granulite, hornblende has the compostion of magnesiohornblende with X_{Mg} = 0.67−0.70. The secondary cummingtonite shows X_{Mg} = 0.67−0.68. Plagioclase has lower anorthite contents of 0.23−0.27 than those in granulite. The hornblende in foliated amphibolite (IK19011404C) is edenitic and has X_{Mg} = 0.61−0.64. The X_{Mg} values of biotite (0.66−0.70) and X_{An} values of plagioclase (0.27−0.30) in this sample are distinct from those in granulite.

Applying the conventional geothermobarometry provides the *P*−*T* conditions of 8−11 kbar, 760−850 °C at the peak, and 5.2−7.8 kbar, 580−640 °C at the retrograde for the granulite (IK19011404A), 650−680 °C at 5 kbar for the leucocratic vein, 4.2−6.5 kbar, 690−720 °C for the amphibolite (IK19011404C). The combination of above *P*−*T* estimations with petrographical features of analyzed samples implies the following thermal history: the assemblage of garnet + orthopyroxene + hornblende + biotite + plagioclase + quartz ± spinel probably was present in the granulite at the peak granulite-facies condition and subsequently the back-reaction with melt might have happened during intial decompression and cooling and caused the partial or complete breakdown of garnet and orthopyroxene into the symplectites. At the upper amphibolite-facies condition, the granulite was affected by the recrystallization like amphibolitization especially at the margin through the intense migmatization and ductile deformation of the host felsic gneiss. The leucocratic vein intruded into a part of the granulite and produced the secondary gedrite after anthophyllite and biotite and secondary anthophyllite after hornblende prior to the later cooling at the amphibolite-facies. The estimated peak *P*−*T* condition of the garnet–orthopyroxene granulite in Oku-iwa rock is comparable with preious reports from the granulite-facies rocks in the transitional zone such as Akarui Point and Tenmondai Rock (e.g., Suzuki & Kawakami, 2019; Shimura et al., 2023). On the other hand, the condition of amphibolitization is similar to the peak one of the amphibolite-facies zone in the northeast LHC (Hiroi et al., 1987). Thus, it may indicate that metamorphic rocks in Oku-iwa Rock underwent the granulite-facies metamorphism prior to the regional amphibolite-facies metamorphism in the amphibolite zone of the LHC. In other words, the timings of peak metamorphic conditions at granulite-facies in the transitional zone and amphibolite-facies in the amphibolite zone might be different. Further petrochronological studies in the LHC are required to clarify the hypothesis.

References

Dunkley, D., Hokada, T., Shiraishi, K., Hiroi, Y., Nogi, Y. and Motoyoshi, Y., Geologica subdivision of the Lützow–Holm Complex in East Antarctica: from the Neoarchean to the Neoproterozoic. Polar Science, 26, 100606, 2020.

Hiroi, Y., Shraishi, K., Yanai, K. and Kizaki, K., Aluminum slicates in the Prince Olav and Sôya Coasts, East Antarctica. Memoirs of National Institute of Polar Research. Special issue, 28, 115-131, 1983.

Hiroi, Y., Shiraishi, K., Motoyoshi, Y. and Katsushima, T., Progressive metamorphism of calc-silicate rocks from the Prince Olav and Sôya Coasts, East Antarctica. Proceedings of the NIPR Symposium on Antarctic Geosciences, 1, 73-97, 1987.

Kitano, I., Toyoshima, T., Ishikawa, M., Katori, T. and Hokada, T. The first report of the occurrence and petrography of garnet-orthopyroxene granulite from Oku-iwa Rock in the Lützow-Holm Complex, East Antarctica. The Eleventh Symposium on Polar Science, Abstract, 2020.

Kitano, I., Hokada, T., Baba, S., Kamei, A., Motoyoshi, Y., Nantasin, P., Setiawan, N.I., Dashbaatar, D., Toyoshima, T., Ishikawa, M., Katori, T. Osanai, Y. and Nakano, N. Zircon geochronology of high-grade metamorphic rocks from outcrops along the Prince Olav Coast, East Antarctica: Implications for the multi-thermal events and regional correlations. Journal of Mineralogical and Petrological Sciences, 118, ANTARCTICA, S009, 2023.

Nakai, Y., Kano, T. and Yoshikura, S., Explanatory text of geological map of Oku-iwa Rock, Antarctica. Antarctic Geologicai Map Series, Sheet 22 Oku-iwa Rock. NIPR, Tokyo, 1981.

Nishi, N., Kawano, Y. and Kagami, H., Rb-Sr and Sm-Nd isotopic geochronology of the granitoid and hornblende biotite gneiss from Oku-iwa Rock in the Lützow-Holm Complex, East Antarctica. Polar Geoscience, 15, 46-65, 2002.

Shimura, T., harada, Y., Fraser, G.L. and Tsuchiya, N. Decompressional spinel + plagioclase symplectite from Tenmondai Rock, Lützow–Holm Complex, East Antarctica: Implications for the garnet–aluminosilicate–spinel–plagioclase geobarometer. Journal of Mineralogical and Petrological Sciences, 118, ANTARCTICA, S008, 2023.

Shiraishi, K., Ellis, D.J., Hiroi, Y., Fanning, C.M., Motoyoshi, Y. and Nakai, Y., Cambrian orogenic belt in East Antarctica and Sri Lanka: implication for Gondwana assembly. Journal of Geology, 102, 47-65, 1994.

Suzuki, K. and Kawakami, T. Metamorphic pressure–temperature conditions of the Lützow–Holm Complex of East Antarctica deduced from Zr–in–rutile geothermometer and Al_2SiO_5 minerals enclosed in garnet. Journal of Mineralogical and Petrological Sciences, 114, 267–279, 2019.

OGo3

High-grade metamorphic rocks distributed in the Instekleppane, Lützow-Holm Complex, eastern part of Dronning Maud Land, East Antarctica

Tatsuro ADACHI[1], Tomokazu HOKADA[2,3], Lakshmanan SREEHARI[4] and Yuki MORI[5]

[1]*Kyushu University,* [2]*National Institute of Polar Research,* [3]*Graduate University for Advanced Studies (SOKENDAI),* [4]*Shimane University,* [5]*Japan Synchrotron Radiation Research Institute*

Eastern part of the Dronning Maud Land, East Antarctica is thought to have been situated in the collision zone between East and West Gondwana during the final stage of amalgamation of the Gondwana supercontinent (e.g., Stern, 1994). Several orogenies explaining the amalgamation of the Gondwana have been discussed: Jacobs and Thomas (2004) proposed East African-Antarctic Orogen (EAAO) which is one huge orogenic belt that was active for a long period (ca. 650-500 Ma), on the other hand, Meert (2003) proposed two crossing orogens where East African Orogen (EAO, Stern, 1994) being active during 750-620 Ma and Kuunga Orogen during 580-500 Ma, however there is no consensus about geological history of the orogenies so far.

Recent studies (Adachi et al., 2023, JMPS; Nakano et al., 2024, JpGU meeting) have found that rocks which experienced metamorphism at ca. 600 Ma are in contact with those formed ca. 550 Ma in several areas, such as Brattnipene in the Sør Rondane Mountains and Bernnabbane in the Lützow-Holm Complex. Based on these findings, the 65th Japan Antarctic Research Expedition (JARE65) conducted a geological survey one of its targets being to reveal the distribution of ca. 600 Ma metamorphic/igneous rocks in the Lützow-Holm Complex, where the main metamorphic event was previously thought to have occurred around 550-530 Ma. A summary of U-Pb ages from the Lützow-Holm Complex (Dunkley et al., 2020) suggests that ca. 600 Ma rocks are likely distributed in the southern part of the Soya Coast, therefore, we conducted a geological survey in that area. In this study, we present a preliminary report on the geology of Instekleppane, where the first multi-day geological survey was conducted by JARE65.

Instekleppane is an exposure approximately 1.5 km × 2.0 km, located in the southernmost part of the Lützow-Holm Bay, on the eastern shore of the Shirase Glacier (Fig. 1). The common lithologies of this exposure are felsic Opx-Cpx-Bt gneiss and felsic Grt-Bt gneiss with mafic to ultramafic Opx-Cpx-Hbl granulite, micaceous Grt-Bt gneiss, Grt-Crd-Bt gneiss and Spr-Crd-Bt gneiss intercalated as layer and lenses (Fig. 2). Grt-bearing rocks are distinctive at the western and the southern parts of this exposure. Among these rocks, Spr-Crd-Bt gneiss (TA2024012401A) has been preliminary analyzed. This rock contains Bt, Crd, Spr and Spl in the matrix with relic Grt, Sil and Opx surrounded by Crd. Qz and Fls are not recognized in the matrix or as inclusions in Grt. Sil and Opx are found as inclusion in Grt. Crd shows intergrowth with Spr ± Spl in the matrix. These observations indicate a change in metamorphic conditions from Grt+Sil+Opx stable condition to Crd+Spr±Spl stable condition, i.e., decompression under *P-T* conditions higher than 950 °C and 0.8 GPa (Harley, 2004). Such change in metamorphic conditions are similar to those reported from several localities in the Lützow-Holm Complex (Rundvågshetta, Yoshimura et al., 2008; Skalvikhalsen, Kawasaki et al., 2013).

In the future, we will analyze the *P-T-t* paths of metamorphic rocks distributed in Instekleppane, particularly focused on differences between Grt-bearing and -free rocks, and also compare *P-T-t* paths of rocks in Instekleppane the with the neibouring exposures in order to discuss geological evolution of Lützow-Holm Complex.

References

Adachi, T., Kawakami, T., Higashino, F. and Uno, M., Metamorphic rocks with different pressure-temperature-time paths bounded by a ductile shear zone at Oyayubi ridge, Brattnipene, Sør Rondane Mountains, East Antarctica, Journal of Mineralogical and Petrological Sciences, 118, Issue ANTARCTICA, 230220, 2023.

Dunkley, D.J., Hokada, T., Shiraishi, K., Hiroi, Y., Nogi, Y. and Motoyoshi, Y., Geological subdivision of the Lützow–Holm Complex in East Antarctica: From the Neoarchean to the Neoproterozoic, Polar Science, 26, 100606, 2020.

Harley, S. L., Fitzsimons, I. C. W. and Zhao, Y. (eds) Antarctica and Supercontinent Evolution. Geological Society, London, Special Publications, 383, 135-167, 2013.

Jacobs, J., and Thomas, R. J., Himalayan-type indenter-escape tectonics model for the southern part of the late Neoproterozoic-early Paleozoic East African-Antarctic Orogen, Geology, 32(8), 721-724, 2004.

Kawasaki, T., Adachi, T., Nakano, N. and Osanai, Y., Possible armalcolite pseudomorph-bearing garnet-sillimanite gneiss from Skallevikshalsen, Lützow-HolmComplex, East Antarctica: Implications for ultrahigh-temperature metamorphism. In:

Meert, J. G., A synopsis of events related to the assembly of the eastern Gondwana, Tectonophysics, 362(1-4), 1-40, 2003.

Nakano, N., Baba, S. and Kagashima, S., Duration of metamorphism in the Bernnabbane from the Lützow-Holm Complex, East Antarctica; significance for microcontinental collision in the Gondwana suture zone, JpGU Meeting 2024, SMP22-07, 2024.

Stern, R.J. Arc assembly and continental collision in the Neoproterozoic East African Orogen: implications for the consolidation of Gondwanaland. Annual review of earth and planetary sciences, 22, 319-351, 1994.

Yoshimura, Y., Motoyoshi, Y. and Miyamoto, T., Finding of sapphirine + quartz association in the sapphirine-bearing garnet-orthopyroxene-sillimanite granulite from Rundvågshetta in the Lützow-Holm Complex, East Antarctica: implication for ultrahigh-temperature metamorphism. In: Satish-Kumar, M., Motoyoshi, Y., Osanai, Y., Hiroi, Y. and Shiraishi, K. (eds) Geodynamic Evolution of East Antarctica: A Key to the East–West Gondwana Connection. Geological Society, London, Special Publications, 308, 371 –391, 2008.

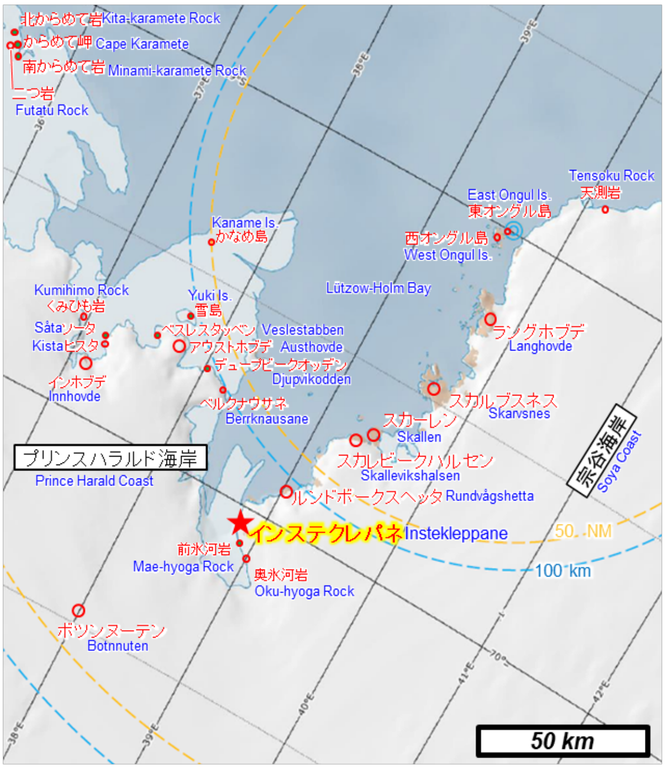

Figure 1. Location of Insteklеppane in the Lützow-Holm Complex.

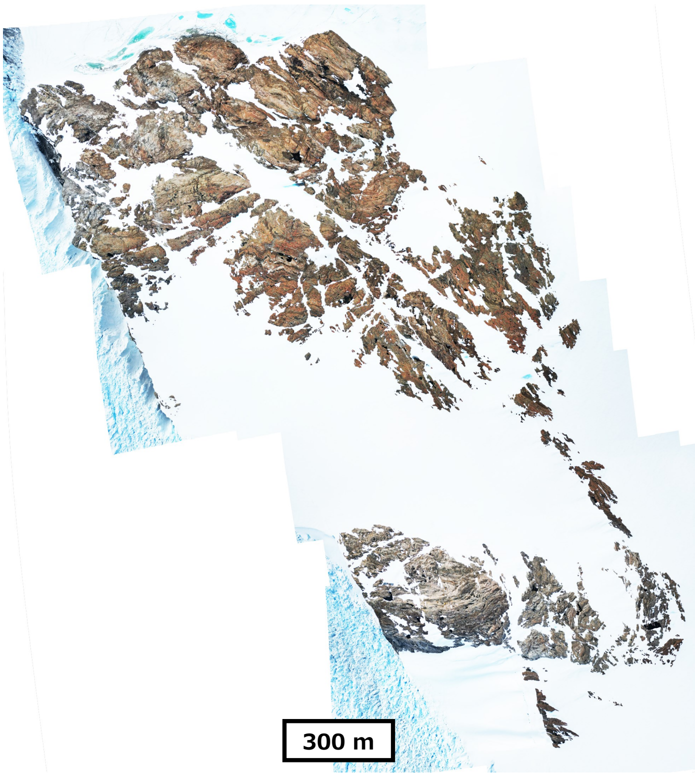

Figure 2. Aearial photo of Instekleppane. Different color indicates different rocktypes. This exposure mainly comprises of Grt-free felsic Opx-Cpx-Bt gneiss (brownish), and Grt-bearing rocks (whitish) are locally distributed at the western and southern part of this exposure.

OGo4

Investigating Natural Radioactivity and Radiogenic Heat Production in the Bedrocks of the Lützow-Holm Complex, East Antarctica

Devika S. Panicker[1], Jun Goto[2], Tomokazu Hokada[3] and Madhusoodhan Satish-Kumar[4]

[1]*Graduate School of Science and Technology, Niigata University, Japan.* [2] *Institute for Research Administration, Niigata University, Niigata, Japan.*

[3] *National Institute of Polar Research, Tokyo 190–8518, Japan.* [4] *Department of Geology, Faculty of Science, Niigata University, Japan.*

This study investigates the natural radioactivity and radiogenic heat production (RHP) within the bedrocks of the Lützow-Holm Complex (LHC) in East Antarctica, a geologically significant region associated with the ancient supercontinent Gondwana. The main sources of heat in the Earth's interior are the heat from the decay of radionuclides such as uranium (U), thorium (Th), and potassium (K).

The LHC forms a part of the Neoproterozoic–Cambrian high-grade metamorphic belt within the East African–Antarctic Orogen, extending along the Prince Harald and Prince Olav Coasts. The rocks in this area, which have undergone amphibolite- to granulite-facies metamorphism during the Late Neoproterozoic to Early Cambrian period (approximately 600–530 million years ago), represent a key area of study for understanding their natural radioactivity. The major rock types include felsic to intermediate orthogneisses (e.g., charnockite, biotite-hornblende gneiss, dioritic gneiss, and meta-granite), metasedimentary rocks (such as pelitic and psammitic gneisses, quartzite, and marble), and metabasites (including mafic granulite, amphibolite, and ultramafic rocks).

The present research focuses on determining the concentration of radionuclides and radiogenic heat production rates. Petrographic analysis and a detailed review of existing geochemical literature reveal that the metamorphic rocks of the LHC, are derived from older igneous formations and are metaluminous to slightly peraluminous rocks characterized by higher concentrations of radionuclides, major oxides and alkalis. We can estimate the average heat production rate from the radionuclides concentration. The average radiogenic heat production rate varies by rock type. For example, granite with 4.6 ppm U, 18 ppm Th, and 33,000 ppm K has a heat production rate of 1050 x 10^{-12} W/kg, while basalt with 0.75 ppm U, 2.5 ppm Th, and 12,000 ppm K has a lower rate of 180 x 10^{-12} W/kg due to its differing elemental concentrations. The radiation levels in rocks can also assessed through the measurement of α-particles, β-particles, and γ-rays emitted during the decay of naturally occurring radionuclides. Among these, gamma radiation is particularly valuable in radio spectrometry surveys, as it can be detected from several hundred meters above the Earth's surface, allowing for remote assessment of radionuclide concentrations. The presence of minerals like K-feldspar, plagioclase, biotite, and trace amounts of radioactive minerals including zircon, and monazite heavily influences the concentration of radionuclides. The rocks targeted for this study, are predominantly enriched with these minerals and those are the various igneous and metamorphic rocks from multiple locations across the LHC, such as Akauri Point, Langhovde, Skarvsnes, Rundvågshetta, Skallevikshalsen, Cape Hinode, Byobu rock, and Gobanme rock. These rock types encompass amphibolite (Hbl + Pl + Qtz + Ap), biotite-amphibolite (Hbl + Bt + Pl + Qtz + Ap), clinopyroxene-amphibolite (Cpx + Hbl + Pl + Qtz + Ttn), biotite-granulite (Cpx + Opx + Bt + Pl + Ap), hornblende-granulite (Opx + Cpx + Hbl + Pl + Qtz), garnet-biotite gneiss (Qtz + Afs + Kfs + Bt + Grt + Zrc + Rt), felsic orthogneiss (Kfs + Pl + Qtz + Bt + Ilm + Hem), granite (Qtz + Kfs + Afs + Bt + Zrc), and granitic gneiss (Qtz + Kfs + Afs + Bt).

Geochemical data from these regions indicate concentrations of radionuclides, particularly U, Th and K. From this data zirconium levels averaged 138.5 ppm across the samples, which might be the reason for enriched U concentration because zircon can accommodate trace amounts of U in its crystal lattice due to their similar ionic radii and charge. The rocks exhibit a peraluminous nature, which can also account for higher concentrations of eTh relative to eU due to monazite, an accessory mineral commonly found in peraluminous rocks. The anomalously high values of K can be due to the high content of feldspar and mica. This study concludes that the elevated radionuclide concentrations in certain rocks are primarily due to the presence of accessory minerals such as zircon and monazite. The rate of radiogenic heat production is also closely linked to the trace element concentrations, with higher levels of Na_2O, K_2O, SiO_2 and total alkali content. Moreover, based on the existing geochemical data, the estimated average heat production rate from these rocks is 640 x 10^{-12} W/kg, with an average U concentration of 0.6 ppm, Th of 2.1 ppm, and K of 30790 ppm, which suggests that these rocks have a typical medium level of radioactive elements, leading to moderate heat production relative to other crustal rocks.

Overall, this research provides critical insights into the natural radioactivity and heat production of the LHC bedrock, highlighting the significant role of Earth's internal heat. Advanced geochemical and radiometric studies are currently underway, and we look forward to presenting the findings at the forthcoming conference.

References

Akingboye, A. S., Ogunyele, A. C., Jimoh, A. T., Adaramoye, O. B., Adeola, A. O. and Ajayi, T, Radioactivity, radiogenic heat production and environmental radiation risk of the Basement Complex rocks of Akungba-Akoko, southwestern Nigeria: insights from in situ gamma-ray spectrometry, Environmental Earth Sciences, 80, 1-24, 2021.

Clauser, C, Radiogenic heat production of rocks, In Encyclopedia of solid earth geophysics, 1304-1310, 2021.

Hokada, T., Satish-Kumar, M. and Kawakami, T, Recent advances in mineralogy, petrology, geochemistry, and geochronology in East Antarctica, Journal of Mineralogical and Petrological Sciences, 119, 2024.

Satish-Kumar, M., Hokada, T., Kawakami, T. and Dunkley, D.J, Geosciences research in East Antarctica (0°E–60°E): present status and future perspectives, Geol. Soc., London, Special Publications, 308(1), 1–20, 2008.

Satish-Kumar, M., Kagashima, S. I., Suda, Y. and Motoyoshi, Y, Geology of Byobu Rock and Gobanme Rock Prince Olav Coast East Antarctica, Polar geosciences, 19, 1-36, 2006.

Suda, Y., Kawano, Y., Yaxley, G., Korenaga, H. and Hiroi, Y, Magmatic evolution and tectonic setting of metabasites from Lützow-Holm Complex, East Antarctica, Geol. Soc., London, Special Publications, 308(1), 211–233, 2008.

Takahashi, K., Tsunogae, T., Santosh, M., Takamura, Y. and Tsutsumi, Y, Paleoproterozoic (ca. 1.8 Ga) arc magmatism in the Lützow-Holm Complex, East Antarctica: Implications for crustal growth and terrane assembly in erstwhile Gondwana fragments, Journal of Asian Earth Sciences, 157, 245–268, 2018.

OGo5

Characteristics and Provenance of Basalts from the Continental Slope off Cape Darnley, East Antarctica: Evidence for Links to the West Antarctic Rift System

Hiroshi Sato[1], Shiki Machida[2] and Masakazu Fujii[3,4]

[1] *Schoool of Business Administration, Senshu University, Kanagawa, Japan*

[2] *Ocean Resources Research Center for Next Generation, Chiba Institute of Technology, Narashino, Japan*

[3] *National Institute of Polar Research, Tachikawa, Japan,*

[4] *Department of Polar Science, School of Multidisciplinary Sciences, SOKENDAI, Tachikawa, Japan*

It is widely recognized that icebergs transport rocks from land, known as ice-rafted debris (IRD) and dropstones, which are closely associated with climate change and the historical dynamics of ice-sheet expansion or extinction in the regions where the icebergs originate (e.g., Ikehara, 2012). However, determining the provenance of these rocks is a significant challenge. Sato et al. (2021) investigated the origin of granitic rocks collected from the Southwest Indian Ridge in the Indian Ocean using petrography, geochemistry, and radiometric dating. They proposed several plausible provenances in Antarctica; however, further refinement is problematic.

During the R/V Hakuho Maru KH-20-1 cruise, a dredging operation was performed on the continental slope off Cape Darnley, East Antarctica. The collected rocks were primarily plutonic and metamorphic and believed to have originated in Antarctica, with some basalts also present. The petrography and geochemistry of the basalts, along with the mineralogy of the mantle xenoliths, were conducted. Based on the major element composition, it is classified as alkaline trachybasalt. Although volcanic rocks are exposed in the vicinity of the collection site, such as at the Jetty Peninsula at the Lambert-Amery Rift and Vestfold Hills at Princess Elizabeth Land, as well as at the Gaussberg volcano, the characteristics of the collected rocks were different. Instead, the trace element composition and isotopic ratios of the sample were similar to those of volcanic rocks of the West Antarctica Rift System (WARS).

The mantle xenoliths in alkaline basalt are harzburgite composed of olivine (60 vol%), orthopyroxene (39 vol%), and clinopyroxene (1.7 vol%). The pressure and temperature conditions of equilibration of the xenoliths, estimated based on mineral phase equilibria, provide crucial insights into the mantle beneath Antarctica. The pressure and temperature estimated from two-pyroxene geothermometry (Putirka, 2008) are approximately 1000°C and 9.0 kbar, respectively. These values are consistent with the geothermal gradient during rifting, as indicated by the xenoliths from the Northern Victoria Land. Based on these features, the basalts are inferred to have originated from the WARS, particularly from the Northern Victoria Land, with significant implications for our understanding of Antarctic geology and tectonics.

References

Ikehara, M., 2012, North-south Shift of Oceanic Fronts in the Southern Ocean: Linkage between Migration of Sea Ice Coverage, Antarctic Polar Front, Antarctic Circumpolar Current, and Global Climate Change from the Present to Late Quaternary: Journal of Geography (Chigaku Zasshi), v. 121, p. 518–535, doi:10.5026/jgeography.121.518.

Putirka, K.D., 2008, Thermometers and barometers for volcanic systems: Reviews in Mineralogy and Geochemistry, v. 69, p. 61–120, doi:10.2138/rmg.2008.69.3.

Sato, H., Machida, S., Senda, R., Sato, K., Kumagai, H., Hyodo, H., Yoneda, S., and Kato, Y., 2021, Petrology, geochemistry, and geochronology of plutonic rocks from the present Southwest Indian Ridge: Implications for dropstone distribution in the Indian Ocean: Polar Science, v. 29, p. 100725, doi:10.1016/j.polar.2021.100725.

OGo6

Decoding paleomagnetic field intensity variations of the Cretaceous Normal Superchron from the Kerguelen Large Igneous Province

Yutaka Yoshimura[1,2], Masakazu Fujii[1,3] , Chie Kato[4] , Osamu Ishizuka[5,6], Kenji Shimizu[6] , and Ryosuke Oyanagi[7]
[1]*National Institute of Polar Research*
[2]*The Institute of Statistical Mathematics*
[3]*The Graduate University for Advanced Studies, SOKENDAI*
[4]*Faculty of Social and Cultural Studies, Kyushu University*
[5]*Geological Survey of Japan, AIST*
[6]*Japan Agency for Marine-Earth Science and Technology*
[7]*Kokushikan University*

The absence of geomagnetic polarity reversals for ~37 million years during mid-Cretaceous period, known as the Cretaceous Normal Superchron (CNS), is a notable phenomenon (Yoshimura, 2022). This extended period can occur by two core-mantle boundary (CMB) heat conditions based on geodynamo simulations: (a) small CMB heat flux (Driscoll & Olson, 2011). (b) recurrent pattern of large and small CMB heat flux is symmetric around equator (Glatzmaier et al., 1999). They yield different geomagnetic field intensity variations. Therefore, paleomagnetic field intensity (paleointensity) of CNS gives us clues to understand the CMB heat condition during CNS. However, two conflict hypotheses of paleointensity variations: (1) strong and stable (Tarduno et al., 2001, 2002), (2) highly variable (Tauxe & Staudigel, 2004; Granot et al., 2007). To reveal the paleointensity during CNS, it is essential to recover 25 or more reliable paleointensity (Tauxe & Staudigel, 2004). Therefore, we plan to use volcanic rocks erupted during CNS such as Kerguelen Plateau and Broken Ridge, known as longest-lived Large Igneous Province (LIP) (Jiang et al., 2021). They were drilled by ODP Legs 119, 120 and 183. It is necessary to analyze paleointensity and rock-magnetic properties combined with lava stratigraphy, geochronology, and geophysical sensing. In this presentation, we introduce how to reconstruct paleointensity variations during CNS using rock samples of Kerguelen Plateau and Broken Ridge drilled by Ocean Drilling Program Leg 183 (Coffin et al., 2002; Frey et al., 2003).

References

Coffin, M. F., Pringle, M. S., Duncan, R. A., Gladczenko, T. P., Storey, M., Müller, R. D., & Gahagan, L. A. (2002). Kerguelen hotspot magma output since 130 Ma. *Journal of petrology*, *43*(7), 1121-1137.

Driscoll, P., & Olson, P. (2011). Superchron cycles driven by variable core heat flow. Geophysical Research Letters, 38(9).

Frey, F. A., Coffin, M. F., Wallace, P. J., & Weis, D. (2003). Leg 183 synthesis: Kerguelen Plateau–Broken Ridge—a large igneous province. In *Proceedings of the Ocean Drilling Program, scientific results* (Vol. 183, pp. 1-48). Texas A & M University Ocean Drilling Program.

Glatzmaier, G. A., Coe, R. S., Hongre, L., & Roberts, P. H. (1999). The role of the Earth's mantle in controlling the frequency of geomagnetic reversals. *Nature*, *401*(6756), 885-890.

Granot, R., Tauxe, L., Gee, J. S., & Ron, H. (2007). A view into the Cretaceous geomagnetic field from analysis of gabbros and submarine glasses. *Earth and Planetary Science Letters*, *256*(1-2), 1-11.

Jiang, Q., Jourdan, F., Olierook, H. K., Merle, R. E., & Whittaker, J. M. (2021). Longest continuously erupting large igneous province driven by plume-ridge interaction. *Geology*, *49*(2), 206-210.

Tarduno, J. A., Cottrell, R. D., & Smirnov, A. V. (2001). High geomagnetic intensity during the mid-Cretaceous from Thellier analyses of single plagioclase crystals. *Science*, *291*(5509), 1779-1783.

Tarduno, J. A., Cottrell, R. D., & Smirnov, A. V. (2002). The Cretaceous superchron geodynamo: observations near the tangent cylinder. *Proceedings of the National Academy of Sciences*, *99*(22), 14020-14025.

Tauxe, L., & Staudigel, H. (2004). Strength of the geomagnetic field in the Cretaceous Normal Superchron: New data from submarine basaltic glass of the Troodos Ophiolite. *Geochemistry, Geophysics, Geosystems*, *5*(2).

Yoshimura, Y. (2022). The Cretaceous normal superchron: a mini-review of its discovery, short reversal events, paleointensity, paleosecular variations, paleoenvironment, volcanism, and mechanism. *Frontiers in Earth Science*, *10*, 834024.

OGo7

The International Seismological Centre (ISC): Products and Services for Polar Regions

Dmitry A. Storchak[1], James Harris[1], Domenico Di Giacomo[1], and the ISC Team[1]
[1]*International Seismological Centre (ISC), United Kingdom*

For over 60 years, the International Seismological Centre (ISC) has been fulfilling its unique mission of producing the most definitive, complete and accurate long-term account of seismicity of the Earth. The ISC data cover the entire period of instrumental seismology from 1904 till present. This work is based on a free and open exchange of parametric event data with several hundreds of seismological institutions, networks and observatories in over hundred countries around the world. The result – the seismological Bulletin of the ISC and several associated datasets that are freely available to all and routinely used by the Geoscience research community and referenced in several hundreds of scientific articles each year.
In this presentation we describe the content of all major ISC datasets in both polar regions: the ISC Bulletin, the International Seismograph Station Registry, the Ground-Truth dataset, the ISC-GEM Global Instrumental Earthquake Catalogue, the ISC-EHB bulletin, the ISC Event Bibliography, the Seismological Dataset Repository, and the ISC Electronic Archive of Printed Station/Network Bulletins.
All of the above datasets are openly available thanks to the financial support of ~75 Member-Institutions in ~50 countries, including four in Japan: JMA, ERI, JAMSTEC and NIPR.

References

International Seismological Centre (2024), On-line Bulletin, https://doi.org/10.31905/D808B830
International Seismological Centre (2024), International Seismograph Station Registry (IR), https://doi.org/10.31905/EL3FQQ40
International Seismological Centre (2024), IASPEI Reference Event (GT) List, https://doi.org/10.31905/32NSJF7V
International Seismological Centre (2024), ISC-GEM Earthquake Catalogue, https://doi.org/10.31905/d808b825
International Seismological Centre (2024), ISC-EHB dataset, https://doi.org/10.31905/PY08W6S3
International Seismological Centre (2024), On-line Event Bibliography, https://doi.org/10.31905/EJ3B5LV6
International Seismological Centre (2024), Seismological Dataset Repository, https://doi.org/10.31905/6TJZECEY
International Seismological Centre (2024), The ISC Electronic Archive of Printed Station/Network Bulletins, https://doi.org/10.31905/GNLY467C

OGo8

Drop and Installation Tests of Antarctic Penetrators Using a Drone and a Helicopter with Operational Seismic and Infrasound Observations

Satoshi TANAKA[1], Takamasa HIRATSUKA[2],Yasuhiro NISHIKAWA[3],Kodai YAMAMOTO[2],

[1] *Department of Solar System Sciences, Institute of Space and Astronautical Science (ISAS), JAXA*

[2] *Aerospace Engineering, Kochi University of Technology*

[3] *School of Systems Engineering, Kochi University of Technology*

We are developing technology to enable the installation of observation sites in the Antarctic region by dropping them from a helicopter, drone, or UAV. Once established, this technology will simplify the process of setting up observation sites, allowing them to be deployed precisely where needed.

This project, which began with the 64th Japanese Antarctic Research Expedition (JARE64) (Nishikawa et al., 2024), is now in its second year. In response to the challenges faced during the first year, we conducted a total of 14 drop and installation tests: six using the drone and eight using the manned helicopter. Additionally, a penetrator designed for practical seismic and infrasound observations was developed and successfully tested.

(1) Drop penetration installation tests

During the JARE64 drone test flight, an anomaly with the magnetic sensor prevented a successful flight. This time, the magnetic sensor was not used, and the navigation system was switched to a dual GPS setup. As a result, the drone was able to fly normally, allowing a penetrator drop installation test to be conducted at S16. Figure 1 shows the condition of the penetrator and the moment it was dropped from 150 meters above the ground.

Figure1. Drone with penetrator (left) and moment of drop from 150 m ground altitude with S16 (right).

Manned helicopter drop tests were conducted at JARE65 using an AS350 helicopter. The helicopter crew included a drop operator, an assistant, and a navigator, who manually released the penetrator by opening the rear seat door above the drop point (Figure 2). The drops were conducted from altitudes of 150 and 400 meters. It was observed that the penetrator's attitude became unstable immediately after the drop at 150 meters and remained unstable at that altitude. However, at 400 meters, the penetrator remained stable and descended almost directly. These tests were conducted over Kitanoura sea ice, Telen, and Langhovde glacier regions, with a total of eight drops performed.

(2) Drop penetration installation and operational testing of actual observation penetrators.

Two of the aircraft dropped from the manned helicopter were equipped with seismic and infrasound sensors, data acquisition equipment, and an Iridium communication system. These were each dropped and installed once on Kitanoura sea ice and Langhovde glacier.

After installation, data is acquired when seismic tremors exceed a certain threshold (using a level-trigger method), and data is transmitted via Iridium communication at set intervals. The computer and communication systems operated normally after the drop installation, and data and commands were successfully transmitted and received. Figure 3 shows an example of an aircraft that penetrated the Langhovde glacier and an example of ice tremor data acquired during a one-week operational test.

Figure 2. The penetrator dropped from an AS350 helicopter at Kitanoura and penetration installation observed from the air.

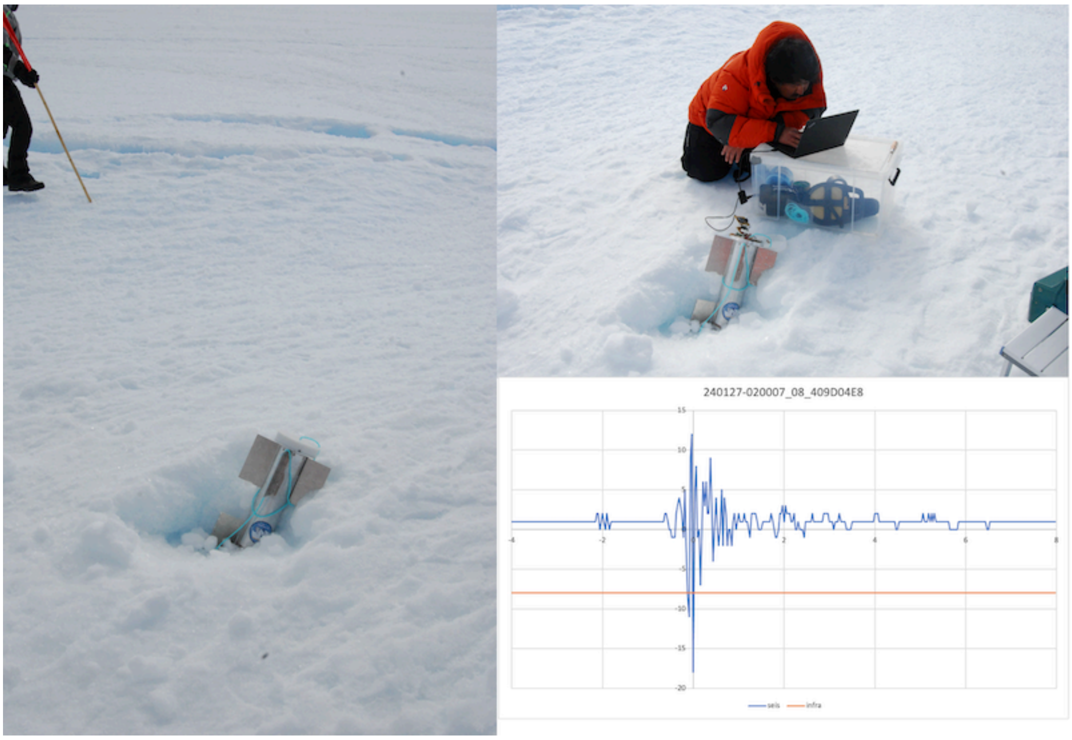

Figure 3: Observation penetrator (left) dropped and installed on Langhovde Glacier. Top right: checking situation after penetration; bottom right: an example of acquired ice quake waveform profile.

Based on the data obtained, we will further improve the hardware and software to enhance their practical application, and they will be deployed in the glacier area for full-scale operational observations by JARE66.

Reference:

1) Nishikawa et al., An introduction to the penetrators for Antarctic regions, The 14th Symposium on Polar Science, 2023

OGo9

Fast-ice observations via an array of wave-ice buoys and the EM-induction sensor during JARE65

Takehiko Nose[1], Yukihide Ishiyama[1], Kohei Mikami[1], Takuji Waseda[1], Kazutaka Tateyama[2], and Tsubasa Kodaira[1]
[1]*Graduate School of Frontier Sciences, The University of Tokyo,* [2]*Kitami Institute of Technology*

Ice-breaking navigation can be hampered by so-called severe ice conditions and affect logistics planning; such a situation adversely disrupts the Japanese Antarctic Research Expedition (JARE). Therefore, knowledge of fast-ice characteristics in the Lützow-Holm Bay (LHB), where Syowa Station is situated, is imperative for summer and winter JARE observations.

Wave-ice buoy deployment

We deployed an array of 21 drifting wave-ice buoys on 28 Dec, 2023 on the LHB face-ice to monitor ice drift during the summer months. In-situ ice thickness was also measured by landing on ice by a helicopter at 16 locations on 4 & 5 Jan, 2024. The buoy positions and ice thickness are displayed in Figure 1.

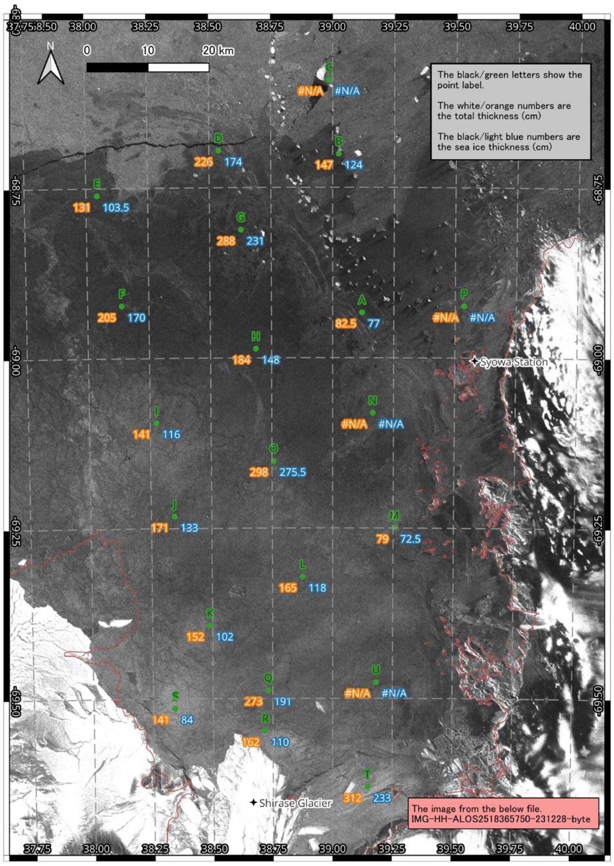

Figure 1: Wave-ice buoys positions on the LHB fast-ice. Sea ice (and total) thickness are also shown at locations where ice-drilling was conducted. The figure also shows the locations of Syowa Station and Shirase Glacier.

There was generally snow depth of more than 20 cm at all positions except for the central-eastern buoys A and M (and Pt. N was deemed too thin to land by a helicopter). Typically, more than 50 % of the snow was snow ice. At 11 of 17 buoy locations, a slush layer was observed below the surface ice. Slush was also observed on the Kitanoura fast-ice (refer to the next section), but this was not the case in JARE64. The difference could imply that sea ice melting progressed faster in 2023/24 than in 2022/23. On 29 Jan, we revisited 5 buoy positions at B, G, F, Q, and R to repeat the thickness measurements. No noticeable reduction in the thickness was observed, except for Pt. R in front of the Shirase Glacier, which thinned by 20—30 cm.

The buoy drifting pattern was examined. Although the fast-ice is typically known to be fastened to land, the majority of buoys were moving northeast at approximately 1.5—2.0 m/day in a steady and consistent manner after the deployment on 28 Dec until 28 Jan. However, the Pt. B and C buoys were stationary. These buoys were located adjacent to a large iceberg (large enough to be easily identified in SAR images); the interpretation here is that the LHB fast-ice was fastened to the iceberg clusters located north of Syowa Station. Another noteworthy observation was that the Pt. R buoy located directly in front of the Shirase Glacier was moving twice as fast as the other buoys; this is consistent with previous observations that Shirase Glacier's front position is moving (e.g., Kondo and Sugiyama, 2023) and a conjecture that the glacier is exerting force on the LHB fast-ice. The drift patterns changed drastically from steady motion to an oscillatory pattern on 29 Jan. We are currently investigating the drift data.

Sea ice thickness measurements via a sled-mounted electromagnetic-induction sensor

To gain more insight into the LHB sea ice properties, we conducted on-ice field observations in Kitanoura located just north of Syowa Station using an electromagnetic-induction (EM) sensor. Apparent conductivity measured by the EM sensor can be used to estimate the ice and ocean interface, and therefore, the ice thickness. An EM sensor mounted on a sled was towed using a snowmobile. In-situ ice thickness was measured by ice-drilling, which can be used to evaluate the sled EM ice thickness accuracy.

We conducted calibration and validation of the EM sensor. In-situ ice thickness was measured at 16 locations. The cal-val location included an area of thin ice located at the downwind side Iwajima (refer to Figure 2 for the Iwajima location). Ice drilling measurements revealed that sea ice thickness part often makes up less than 50 % of the total ice thickness, i.e., snow including slush can be the major part of the ice profile. Note that sea ice thickness is an indirect measurement that subtracts the snow part that may consist of soft (scrapable) snow, slush layer, and snow ice. At one location where the puddle underneath the surface snow ice was visible, the sea ice thickness was estimated as 3 cm with the surface snow ice being 27 cm (and slush = 67 cm).

The key outcome of the cal-val exercise was that the JARE65 calibration values were generally consistent with the existing calibration from many years ago (aka the look-up table). The sensitivity of the sled-EM sensor to distinguish the multi-year ice and the first-year ice was demonstrated when we overlaid the sled-EM estimated thickness with that of Kitanoura's minimal sea ice extent in 2023 taken by Landsat on 26 Mar 2023 as shown in Figure 2. We conjecture that the EM-estimated ice thickness is accurate within +-30cm; the results here suggest the sled-EM could be used for fast-ice reconnaissance activities by being able to detect thin ice.

We will present updated results and analysis of sea ice thickness and buoy drift observations from JARE65.

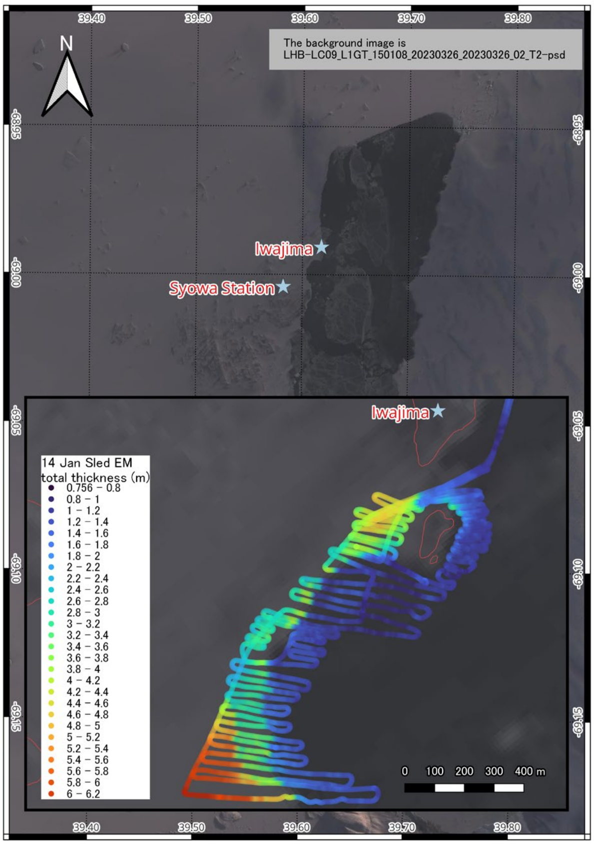

Figure 2: Sled EM ice thickness measured on 14 Jan, 2024 overlaid on the 26 Mar Landsat image when Kitanoura's minimum sea ice extent in 2023 was captured. Note: the Landsat image is dark likely because of lack of light at this time of the year.

Reference

Kondo K, Sugiyama S. Calving, ice flow, and thickness of outlet glaciers controlled by land-fast sea ice in Lützow-Holm Bay, East Antarctica. Journal of Glaciology. Published online 2023:1-13. doi:10.1017/jog.2023.59

OGo10

Seismic imaging of the crust and lithospheric mantle of the Pan-African mobile belt, the Lützow-Holm Complex, East Antarctica

Masaki Kanao[1], Shigeru Toda[2] and Masahiro Ishikawa[3]
[1] *National Institute of Polar Reseaarch*
[2]*Aichi University of Education*
[3]*Yokohama National University*

The Lützow-Holm Complex (LHC) experienced regional metamorphism in the early-Paleozoic age (Shiraishi et al., 1994). Metamorphic grade increases progressively from the Prince Olav Coast (amphibolite facies) to the Sôya Coast (granulite facies) and the maximum thermal axis runs through the southern part of the Lützow-Holm Bay with an NNW-SSE striking direction (Ishikawa et al., 1994). The transition zone between amphibolite facies and granulite facies is in the central part of the LHC and is defined as the first appearance of orthopyroxene in ordinary basic to intermediate gneisses. During this metamorphic event, the LHC was deformed under compressional stress perpendicular to the thermal axis (almost parallel to the coast) as part of the Pan-African orogeny. The Dronning Maud Land, located to the west of LHC, was once connected to the Kaapvaal Craton (Nkosi et al., 2022; Fujita et al., 2024) during the time of the Gondwana supercontinent. Investigating and comparing the crustal structures and evolutionary processes around the cratons of both East Antarctica and South Africa is crucial for studying the formation and breakup processes of the supercontinent that once spanned the southern hemisphere in Earth's history (Brown et al., 2001).

Apart from monitoring observations at Syowa Station in the northern part of the LHC, artificial seismic surveys aimed at elucidating the structure of the crust and uppermost mantle were conducted on the continental ice sheet of LHC under the SEAL (Structure and Evolution of the Antarctic Lithosphere) project (Kanao et al., 2004) by JARE-41 and JARE-43 (2000 and 2002 summer seasons). Detailed velocity structures were derived through refraction and wide-angle reflection surveys using large-scale explosive sources, and the velocity structure of the continental ice sheet, including the firn layer, was also determined (Miyamachi et al., 2003; Yoshii et al., 2004). Additionally, architectures of the deep reflective sections were imaged through reflective method analysis (Tsutsui et al., 2001; Yamashita et al., 2006). The obtained crustal and lithospheric mantle structures were integrated with separately surveyed geological information and geophysical data to consider lithospheric formation patterns that contain rock deformation and flow mechanism. This integration also explored the large-scale and deep-seated tectonic variations of the LHC related to the formation and breakup of the Gondwana, such as the Pan-African orogeny (Ishikawa and Kanao, 2002; Kanao et al., 2011). Furthermore, density structures of the crust and upper mantle were demonstrated based on gravity measurements along the seismic survey lines on the Mizuho Plateau (Toda et al., 2013, 2014).

After the SEAL project, no large-scale artificial seismic structural surveys have been conducted by JAREs, but preliminary experiments using simple near-vertical reflection methods, such as free-fall weights, were carried out in the outcrop areas of East Ongul Island, where Syowa Station is located, by JARE-48 (2007) and JARE-51 (2010), respectively. These surveys contributed to understand the layered structure of the gneiss that makes up the surface layer of the LHC, as well as to estimating the position of faults and fracture zones deep underground near the Ongul Strait (Kanao et al., 2014). However, these two surveys did not achieve detailed imaging of the geological structures because of the coarse interval between observation points and the low number of stackings (repetition of signals) which resulted in low seismic source energy. In this regard, explorations in JARE-48 and JARE-51 remained preliminary experiments for future comprehensive reflection surveys.

In the coastal outcrop areas in the LHC, we are planning to conduct shallow crustal reflection seismics and surface wave surveys by deploying dense seismic station by 10 m interval with using small but highly energy-efficient active seismic sources (PASS; Tsuji et al., 2021) in near future. By scheduling at least one week of observations in each outcrop, sufficient stacking (repetition of signals) will be achieved. This is expected to improve the S/N ratio and spatial resolution, allowing for more detailed reflection profiles and velocity structures than those obtained in previous surveys. These surveys aim to elucidate the geological structure boundaries and deeper structures at specific target locations within each outcrop area. In some of the outcrop areas (Skarvsnes), ground soil monitoring using the PASS sources is planned to target sedimentary layers distributed over the basement rocks. This will estimate the amount of change in seismic velocity due to the thawing and freezing of the permafrost in the subsurface depths during the Antarctic summer seasons (as comparison with by Tsuji et al., 2012).

Furthermore, temporary observation stations with portable broadband seismometers will be established for data collection, and surface rock samples will be collected near the seismic survey lines. The data from temporary observations with broadband seismometers will be used to obtain the distribution of the local shallow crustal velocity structure through seismic noise interferometry. By integrating these data (reflection profiles, velocity models, and rock elastic wave velocities), we aim to estimate the geological structure boundaries in the shallow crust of each outcrop area and the spatial distribution of seismic wave velocities related to structural heterogeneities. Based on the findings from previous geological surveys and the results of large-scale deep structure surveys conducted by the SEAL, we may be able to discuss in detail the evolutionary processes of the upper crust in the outcrop areas of LHC in relation to the formation and breakup processes of the Gondwana supercontinent.

References

Brown, L. D., Kroner, A., Powell, C., Windley, B. and Kanao, M., Deep Seismic Exploration of East Gondwana: the LEGENDS Initiative, Gondwana Research, 4, 846-850, 2001.

Fujita, K., H. Ogasawara, Y. Yabe, R. Tadokoro, K. Suzuki, S. Horiuchi, M. Naoi, M. Manzi, R. Durrheim, B. Liebenberg, v. H. Esterhuizen, M. Kanao and the DSeis team, The seismogenic zone of the 2014 Orkney M5.5 earthquake, South Africa, SEISMIX 2024, Uppsala, Sweden, 24-28 June, 2024.

Ishikawa, M., Motoyoshi, Y., Fraser, G. L. and Kawasaki, T., Structural evolution of Rundvågshetta region, Lützow-Holm Bay, East Antarctica, Proceedings of the NIPR Symposium on Antarctic Geosciences, 7, 69 – 89,1994.

Ishikawa, M. and Kanao, M., Structure and collision tectonics of the Pan-African orogeny, Scientific Report, Earth. Res. Inst., 77, 165-180, 2002 (in Japanese)

Kanao, M. and M. Ishikawa, Origins of the Lower Crustal Reflectivity in the Lützow-Holm Complex, Enderby Land, East Antarctica, Earth Planets Space, 56, 151-162, 2004.

Kanao, M., A. Fujiwara, H. Miyamachi, S. Toda, M. Tomura, K. Ito and T. Ikawa, Reflection imaging of the crust and the lithospheric mantle in the Lützow-Holm Complex, Eastern Dronning Maud Land, Antarctica, derived from the SEAL Transects, Tectonophysics, 508, 73-84, 2011.

Kanao, M., T. Takemoto, A. Fujiwara, K. Ito and T. Ikawa, Shallow reflection surveys of the East Ongugl Island, the Lützow-Holm Complex, East Antarctica, Int. J. Geosci., 2014, 1037-1047, 2014.

Miyamachi, H., S. Toda, T. Matsushima, M. Takada, A. Watanabe, M. Yamashita and M. Kanao, Seismic refraction and wide-angle reflection exploration by JARE-43 on Mizuho Plateau, East Antarctica, Polar Geosci., 16, 1-21, 2003.

Nkosi, N. Z., Manzi, M. S. D., Westgate, M., Roberts, D., Durrheim, R. J., Ogasawara, H., Ziegler, M., Rickenbacher, M., Liebenberg, B., Onstott, T. C. and the DSeis team, Physical property studies to elucidate the source of seismic reflectivity within the ICDP DSeis seismogenic zone: Klerksdorp goldfield, South Africa, Int. J. Rock Mech. Min. Sci., 155, 2022.

Shiraishi, K., Ellis, D.J., Hiroi, Y., Fanning, C.M., Motoyoshi, Y. and Nakai, Y., Cambrian orogenic belt in East Antarctica and Sri Lanka: implication for Gondwana assembly, J. Geol. 102, 47–65, 1994.

Toda, S., H. Miyamachi, H. Murakami, T. Tsutsui and M. Kanao, Gravity survey along the Mizuho traverse routes, East Antarctica: SEAL seismic exploration in 1999-2000, Inter. J. Geosci., 2013, 1392-1400, 2013.

Toda, S., H. Miyamachi, M. Kanao, T. Matsushima, M. Takada, A. Watanabe and M. Yamashita, Gravity survey on the Mizuho Plateau, East Antarctica: SEAL seismic exploration in 2001-2002, Inter. J. Geosci., 2014, 146-155, 2014.

Tsuji, T., T.A. Johansen, B.O. Ruud, T. Ikeda and T. Matsuoka, Surface-wave analysis for identifying unfrozen zones in subglacial sediments, GEOPHYSICS, 77, EN17-EN27, doi:10.1190/geo2011-0222.1, 2012.

Tsuji, T., T. Ikeda, R. Matsuura, K. Mukumoto, H.F. Lawrens, T. Kimura, K. Yamaoka and M. Shinohara, Continuous monitoring system for safe managements of CO_2 storage and geothermal reservoirs, Scientific Reports, Nature, 11, 19120, doi:10.1038/s41598-021-97881-5, 2021.

Tsutsui, T., M. Yamashita, H. Murakami, H. Miyamachi, S. Toda and M. Kanao, Reflection profiling and velocity structure benearth Mizuho traverse route, East Antarctica, Polar Geosci., 14, 212-225, 2001.

Yamashita, M., H. Miyamachi, M. Kanao, T. Matsushima, S. Toda, M. Takada and A. Watanabe, Deep Reflection Imaging beneath the Mizuho Plateau, East Antarctica, by SEAL-2002 Seismic Experiment, In: Futterer D. K., D. Damaske, G. Kleinschmidt, H. Miller, and F. Tessensohn (Eds), Antarctica: Contributions to global earth sciences, Springer-Verlag, Berlin Heidelberg New York, 147-154, 2006.

Yoshii, K., K. Ito, H. Miyamachi and M. Kanao, Crustal structure derived from refractions and wide-angle reflections in the Mizuho Plateau, East Antarctica, Polar Geosci., 17, 112-138, 2004.

OGo11

GPS-time synchronized surface-tunnel-borehole seismic surveys for deep mineral exploration

Musa S.D. Manzi[1], Alireza Malehmir[2], Laura V. Socco[3], Raymond J. Durrheim[1]
[1]*University of the Witwatersrand, Johannesburg, South Africa*
[2]*Uppsala University, Sweden*
[3]*Politecnico di Torino, Italy*

Energy transition from fossil fuels to green-type technologies is more than ever accelerated. This is evident as government organisations, mineral and mining sectors push enormously to accelerate this transition with subsidies and more research possibilities. There is, however, a major obstacle that alternative sources of energy require access to raw materials for generation, storage and transportation. The mineral exploration industry continues to chase deep-seated deposits in hardrock environments while making sure intermediate ones are also effectively explored using state-of-the-art technologies that are environmentally friendly and cost-effective, but also provide sufficient resolution for drilling programmes. As demand increases, the mining industry also faces an increasing push to produce more raw materials in more challenging mining environments prone to seismicity and characterized by complex geological structures. Geophysical methods, seismic methods in particular, are getting more attention than ever to address these challenges because they provide high-resolution images of key subsurface geological structures and relatively retain their resolution at target depths.

This paper addresses these challenges and provides several solutions. Beyond the state-of-the-art seismic solutions for deep-seated mineral deposit targeting are presented through case studies from a deep mine site (> 3 km depth below ground surface) in the Witwatersrand Basin (South Africa). Firstly, we showcase the state-of-the-art surface-tunnel-borehole solutions developed under the EU-funded Eramin Future project for shallow and deep-seated mineral deposit targeting. Secondly, we discuss the current status and limitations of geophysical methods in difficult underground mining environments (e.g., lack of GPS time signal) and present our newly developed solutions for in-mine (~ 3 km mine tunnel) seismic surveys that can be utilised to image the mineral deposits and complex geological structures several metres ahead of the mine face, and metres-to-kilometres below and above the tunnel floor. Essentially, these new in-mine seismic solutions take advantage of the distributed acoustic sensing (DAS) technology that incorporates fiber-optic cables and wireless seismic recorders, which are then GPS-time synchronised using a newly developed GPS-time transmitter system developed under the Smart Exploration project (Figure 1). The GPS time transmitter opens up new opportunities in exploration projects as it allows the recording of seismic data in GPS-denied environments such as in-mine infrastructure (e.g., mine tunnels and underground boreholes).

In 2023, innovative surface and in-mine seismic surveys (Figure 1) were conducted at South Deep gold mine in South Africa to evaluate the effectiveness of employing broadband nodal sensors, cabled systems and fiber optic cables for deep mineral exploration in a challenging active mining environment. The 2D/3D surface seismic surveys employed a combination of co-located broadband micro-electromechanical sensors (MEMS), 3-component recorders (10 Hz), 1-component recorders (10 Hz), and distributed acoustic sensing (DAS) for comparison purposes. A 6-ton broadband seismic vibrator using 2-200 Hz linear sweeps was used as an energy source. The surface seismic survey successfully imaged the deep-seated gold-bearing horizon (VCR-Ventersdorp Contact Reef) and associated geological structures such as faults and dykes, which are critical for future mine planning and development. in-mine seismic surveys employed a combination of co-located DAS (distributed acoustic sensing) cables and cabled geophones (14 Hz), and employed a 500 kg drophammer as an energy source. In addition, the DAS cable was instrumented into a 65 m-long horizontal exploration borehole to record active and passive data. The tunnel-borehole DAS array was also synchronised with the surface arrays using a GPS-time transmitter (Figure 1a,b) developed by Malehmir et al. (2029). The workflow used in the tunnel study includes (1) survey design and data acquisition, (2) computation of the P-wave refraction tomogram, (3) conventional seismic data processing, (4) data analysis using surface attributes using the approach by Colombero et al. (2019), and (5) data conditioning and interpretation using complex-trace seismic attributes described by Manzi et al. (2012). The tunnel seismic survey was successful in the delineation of geological structures that crosscut and displace the gold orebody by several meters above the tunnel floor (Figure 2a,b). Despite the enormous challenges encountered around the logistics in an operating world-class deep gold mine, we managed to generate over 200 time-tagged shots in the mining tunnel and we used the time tags from the recording device to harvest data from the nodal recorders operating autonomously on the surface array. Our novel approach is opening new possibilities for more innovative surface-tunnel-borehole seismic survey designs for mineral exploration in challenging and noisy mining environment.

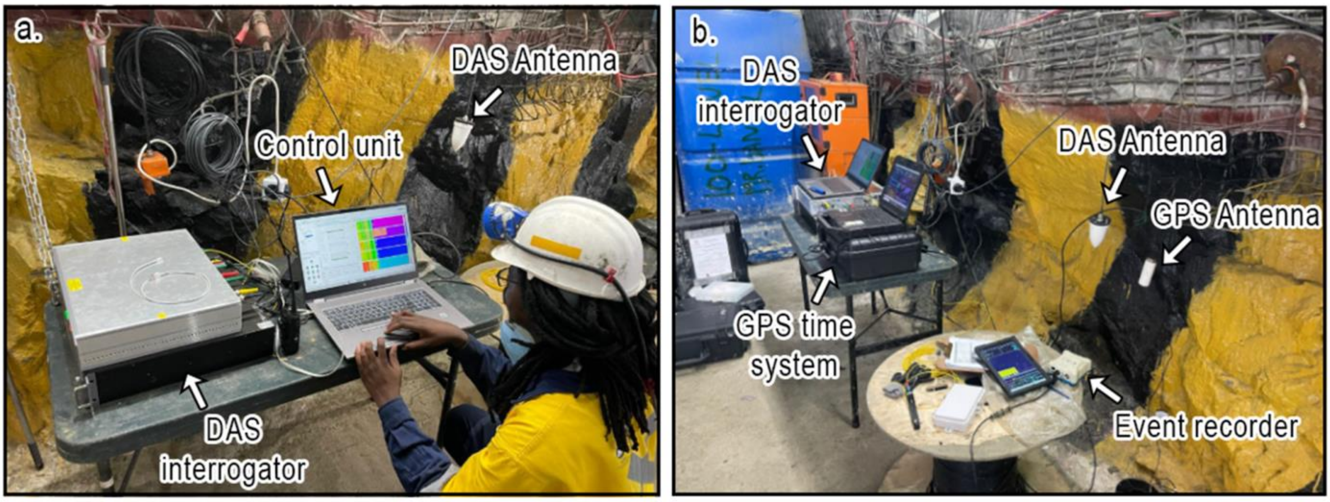

Figure 1. The tunnel seismic set-up showing the DAS (distributed acoustic sensing) interrogator (a) and the GPS time system, GPS antenna, and recording device (b).

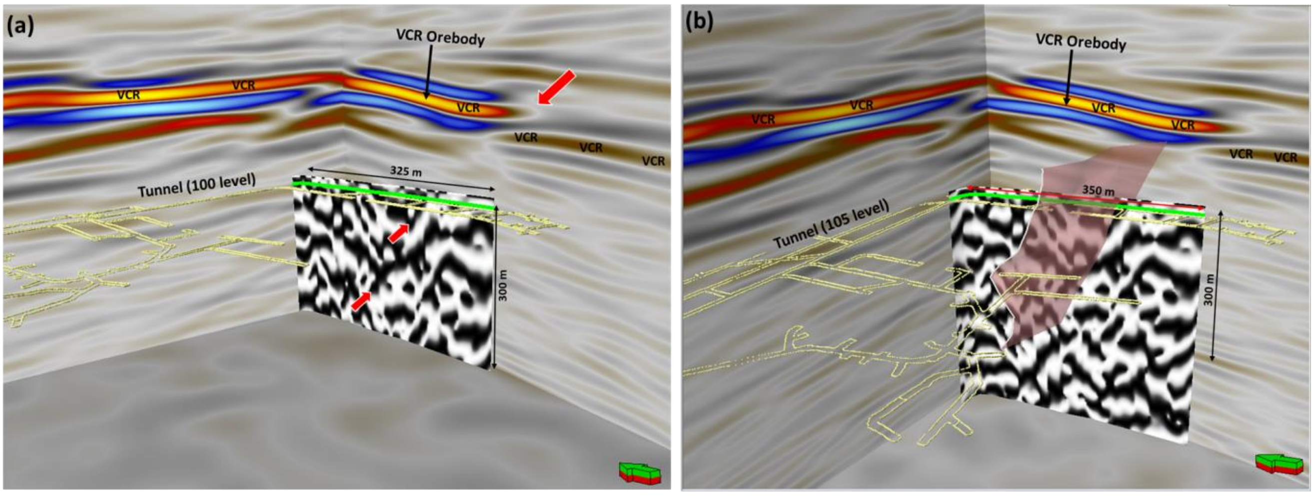

Figure 2. The tunnel seismic survey results from the cabled seismic system showing the imaging of the fault crosscutting the orebody (VCR-Ventersdorp Contact Reef) and the mine-mapped structure overlaid on the tunnel seismic section (b).

References

Colombero, C., C. Comina, and L.V. Socco, Imaging near-surface sharp lateral variations with surface-wave methods – Part 1: Detection and location. Geophysics, 84(6), 93-111, 2019.

Malehmir, A., L.Dynesius, and T. Sjölund, Mining and mineral exploration system and methods for performing time-accurate measurements in a mine. Patent (Swedish Intellectual Property Office, granted on 17-11-2020), SE 543 288 C2, 2019.

Manzi, M.S.D., M.A.S. Gibson, K.A.A. Hein, N. King, and R.J. Durrheim, Application of 3D seismic techniques to evaluate ore resources in the West Wits Line goldfield and portions of the West Rand goldfield, South Africa. Geophysics, 77, 163–171, 2012.

OGo12

An M5.5 earthquake on a lamprophyre dyke crosscutting West Rand Group (3.5-7 km depth range) in Witwatersrand Supergroup (2.97-2.80 Ga)

Hiroshi Ogasawara[1] and the DSeis team[2]

[1]*Ritsumeikan University*

[2]*https://www.ritsumei.ac.jp/~ogasawar/DSeis/TheDSeisTeam20230708.pdf*

We report on an ICDP drilling project (2016-ongoing) that probed the aftershock zone of the 2014 Orkney M5.5 earthquake (hereafter Orkney M5.5 earthquake, a star in Figure 1), South Africa, where ICDP is an abbreviation of the International Continental Scientific Drilling Program with UNESCO as a liaison member. Drilling in the aftershock zones of the M5.5 Orkney earthquake was part of the DSeis project that drilled in the M2.0-5.5 seismogenic zones in deep South African gold mines. The Orkney earthquake and its aftershocks ruptured almost the entire depth range of the West Rand Group (3.5-7 km depth range; red vertical line in Figure 1) by left-lateral strike-slip faulting below the Moab Khotsong mine.

The DSeis project site at the Moab Khotsong Mine (star in Figure 1) is located on the northern margin of the Karoo Supergroup on the current surface geological map, but 2.9 km below surface (Figure 2) in the uppermost formation of the West Rand Group (red line in Figure 1). The West Rand Group (mainly marine shale and quartzite with 2.914 Ga basaltic andesite lava) is overlain by the Central Rand Group, which hosts the economic gold reef, with both groups forming the Witwatersrand Supergroup. The Witwatersrand Supergroup is overlain by Ventersdorp LIP lava and crosscut by numerous NE-SW normal faults, dikes, sills as the rift structure (blue arrows) formed. The Ventersdorp LIP corresponds in age to the Fortescue Group of the Pilbara Craton in northwestern Australia, both of which were once part of the Gondwana supercontinent. During the post-LIP period, the Transvaal Supergroup with dolomite formation formed. After Bushveld and Karoo age activity, with repeated subsidence and uplift with erosion, the present surface is a paneplane at about 1300m altitude at the Moab Khotsong mine.

The drilling provided us with a rare opportunity to elucidate the interaction between the Archean meta-sedimentary hard rock formation and the intrusives over several generations (Figure 1a) through integrated analysis of samples from full core drilling (Figure 2; Ogasawara et al. 2019, 2020, 2024; Miyamoto et al. 2022), borehole logging (e.g., Nkosi et al. 2022), brine analysis (e.g., Nisson et al. 2023), the legacy 3D seismic reflection survey data (Fujita et al. this symposium), HypoDD relocated aftershocks (Fujita et al. this symposium), and friction tests (Yabe et al., 2024). Yabe et al. (this symposium) will describe a follow-up drilling project. Thus, we focus on documenting what Fujita et al. and Yabe et al. (this symposium) do not report.

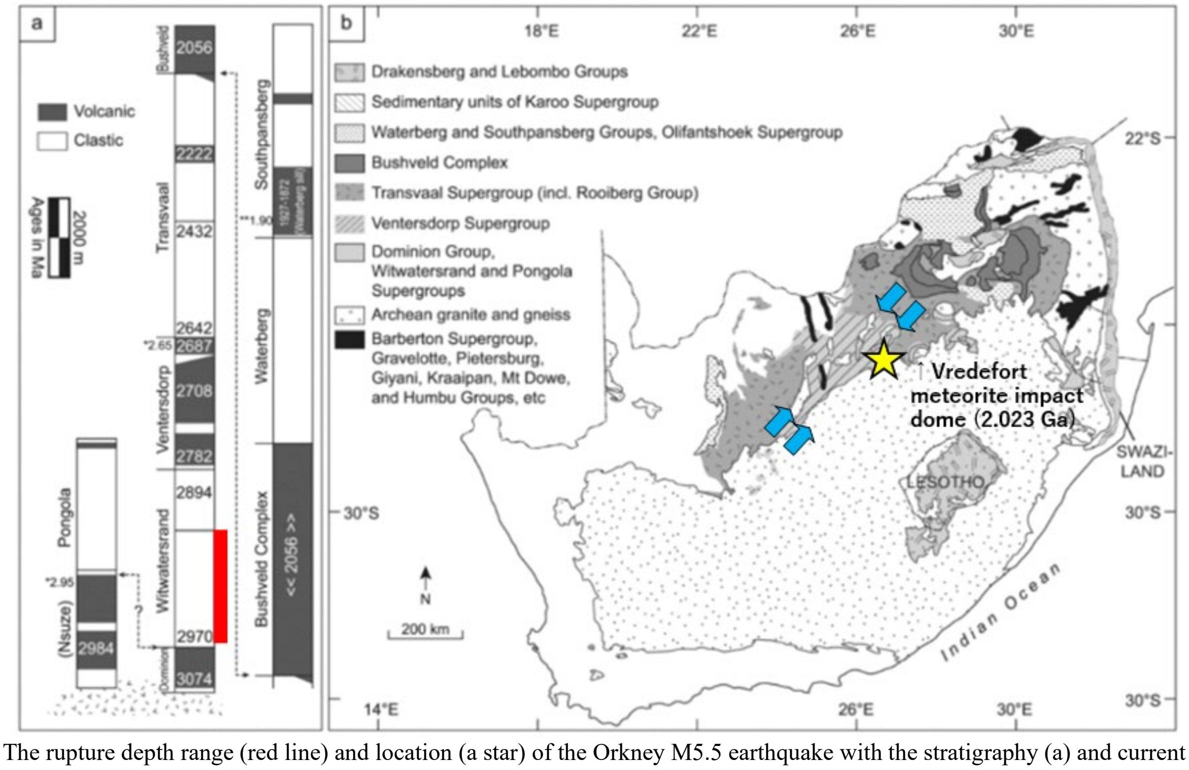

Figure 1 The rupture depth range (red line) and location (a star) of the Orkney M5.5 earthquake with the stratigraphy (a) and current surface geology (b) in South Africa (modified from Figure 6.1 of Ernst, 2014). Arrows indicate the rift axis of the Ventersdorp Large Igneous Province.

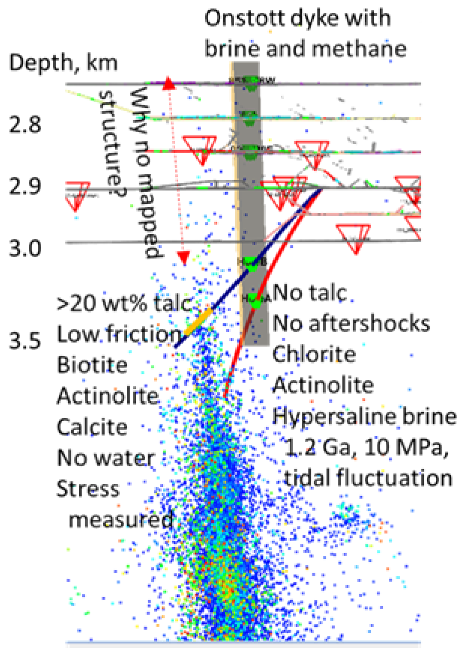

Figure 2 Illustrative summary of DSeis drilling and results. In-mine seismic stations (▽) along the horizontal tunnels from 2.6 to 3.1 km depth precisely delineated the aftershocks of the Orkney M5.5 earthquake. To target the aftershocks, the DSeis project commenced full-core drilling from 2.9 km depth in the uppermost formation of the West Rand Group. The drilling intersected the metasedimentary formations and sills that dip 20 degrees to the southeast, as well as some dikes. Where the drilling intersected the aftershock plane, the ultramafic lamprophyre dyke (initially intact core followed by fault breccia and gouge) was recovered (Ogasawara et al. 2019). Approximately 300 m east of the lamprophyre dyke, another dyke was recovered that was more mafic than the dolerite but less mafic than the lamprophyre dyke. This dyke, which we have named the Onstott dyke in honor of his discovery of 1.2 Ga hypersaline brine (Warr et al. 2022; Nisson et al. 2023), has not hosted aftershock activity, although it is nearly parallel to the lamprophyre dyke. Mineral composition, especially the presence of talc (Miyamoto et al. 2022; Yabe et al. 2024), appears to control the seismic characteristics of these dykes.

References

Ernst, R.E., Large Igneous Provinces, Cambridge University Press, 2014.

Miyamoto, T. et al., Characteristics of Fault Rocks Within the Aftershock Cloud of the 2014 Orkney Earthquake (M5.5) Beneath the Moab Khotsong Gold Mine, South Africa, Geophysical Research Letters, 49(14) e2022GL098745, DOI: 10.1029/2022GL098745, 2022.

Nisson, D.M. et al., Hydrogeochemical and isotopic signatures elucidate deep subsurface hypersaline brine formation through radiolysis driven water-rock interaction, Geochimica et Cosmochimica Acta. 340, 65-84, DOI: 10.1016/j.gca.2022.11.015, 2023

Nkosi, N.Z. et al., Physical property studies to elucidate the source of seismic reflectivity within the ICDP DSeis seismogenic zone: Klearksdorp goldfield, South Africa, International Journal of Rock Mechanics and Mining Sciences, 155, DOI: 10.1016/j.ijrmms.2022.105082 2022.

Ogasawara, H. et al., 2019 status report: Drilling into seismogenic zones of M2.0–M5.5 earthquakes in South African gold mines (DSeis project), Proc. 9th International Congress on Deep and High Stress Mining, Southern African Institute of Mining and Metallurgy, 375-384. DOI: 10.36487/ACG_rep/1952_28_Ogasawara, 2019.

Ogasawara, H. et al., The seismogenic zones of an M2.0-5.5 earthquakes successfully recovered in deep South African gold mines: the outcomes and the follow-up plan. Europ. Geophys. Union 2020, EGU2020-12094, DOI: 10.5194/egusphere-egu2020-12094, 2020.

Ogasawara, H., et al., From DSeis to PROTEA - Probing the heart of an earthquake, especially the interaction between metasedimentary rocks and mantle-derived intrusions. EGU General Assembly 2024, Vienna, EGU24-14233, DOI: 10.5194/egusphere-egu24-14233, 2024

Warr, O. et al., ^{86}Kr excess and other noble gases identify a billion-year-old radiogenically-enriched groundwater system, Nature Communication, 13, Article number: 3768, DOI: 10.1038/s41467-022-31412-2, 2022.

Yabe, Y. et al., Frictional properties of the fault hosting aftershocks of the 2014 Orkney earthquake (M5.5), South Africa, and proposal of a new drilling project PROTEA to probe the heart of the earthquake, EGU General Assembly 2024, EGU24-3723, DOI:10.5194/egusphere-egu24-3723, 2024.

OGo13

Spatial variation in seismic velocity for the dykes recovered in deep seismogenic zone, the Kaapvaal craton in South Africa

Kaoru Fujita[1], Hiroshi Ogasawara[2], Yasuo Yabe[3], Yuhji Yamamoto[4], Masaki Kanao[5], Junichi Okuno[5],

[1]The Graduate University for Advanced Studies, [2]Ritsumeikan University, [3]Tohoku University, [4]Marine Core Research Institute, Kochi University, [5]National Institute of Polar Research

The southern part of African continent is known to be stable with extant several Pre-Cambrian terrains including the Kaapvaal craton, however, recent tectonic and magmatic dynamics have affected to the formation of the current crustal structure. Several gold fields in the Kaapvaal craton are mined from the surface to 3 km below it, making it an opportune area for understanding the subsurface phenomena. In 2014, a M 5.5 earthquake occurred just below the Moab Khotsong gold mine located on the outskirts of Orkney, South Africa. The fault rupture zone caused by the main and aftershocks ranged from 3.5 to 7 km in depth, with the upper edge several hundred meters below the deepest tunnel in the mine. It proved to be within drillable range from the deepest level of the mine and the International Continental Scientific Drilling Program (ICDP) accepted the project "Drilling into seismogenic zones of M2.0-5.5 earthquakes in South African gold mines (DSeis)" in 2016. The DSeis drilled from a 2.9 km underground tunnel to directly observe the seismogenic zones (Ogasawara et al. 2019). We full-core drilled Holes A, B, and C for a total length of 1.6 km (Fig. 1a). We will report on our seismic velocity measurements at intervals of a few centimeters along the recovered samples from the two different dykes, one of which hosted the aftershocks (ultramafic lamprophyre; a blue rectangle in Fig.1b) with fault gouge zone and core loss but the other (mafic dyke; a red rectangle) did not. We compare variations in density, magnetic susceptibility and CT values along the cores to investigate into the effects of rock alteration metamorphism.

Within the Lamprophyre dyke, the velocity decreased from 6.0 km/s to 5.0 km/s in a section of about 2 m toward the core loss zone. This was common to both Hole B and C. On the other hand, no significant velocity change was observed in the mafic dyke, which intrudes quartzite (metamorphic sedimentary rocks). These results are compared with the density and porosity data to discuss spatial velocity changes within two dykes. In the presentation, we will compare these results of velocity variations with the magnetic susceptibility, CT values and acoustic impedance calculated by assuming lithologic layering in these dykes. This detail investigation will give a unique information on the creation of seismogenic zones in the stable Archaean cratons.

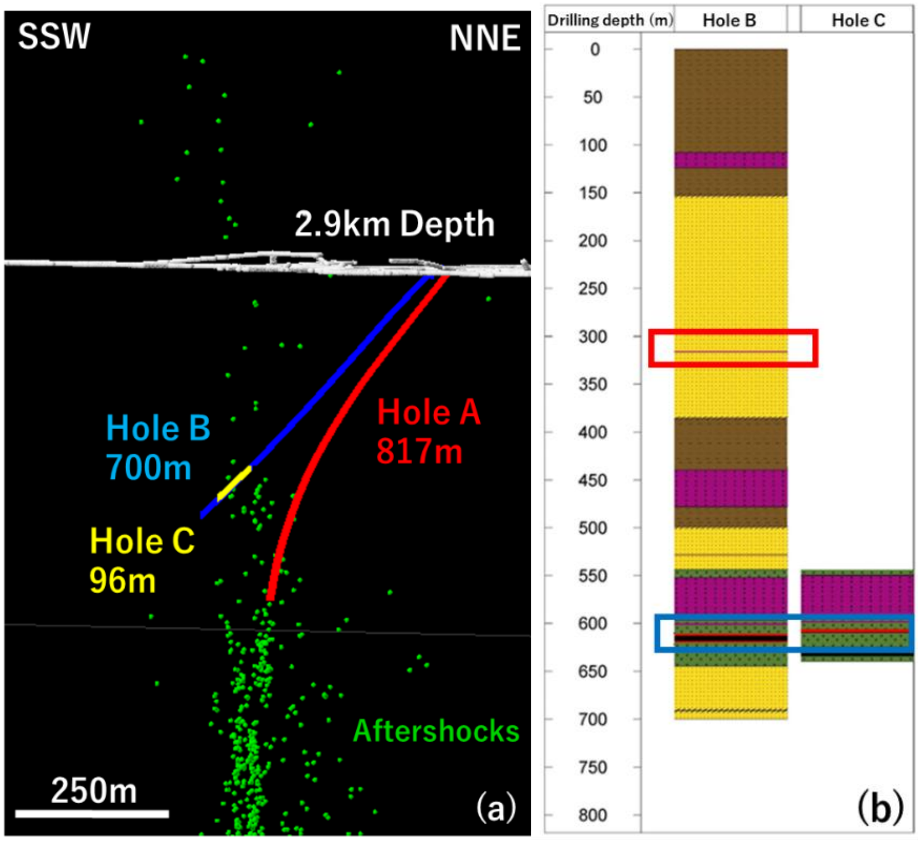

Fig. 1
(a) Location of the 2.9 km underground tunnel and the DSeis boreholes. Red line is Hole A, blue line is Hole B, and yellow line is Hole C. Green dots are some aftershocks HypoDD relocated by Tadokoro 2020. (b) The lithology of Holes B and C. Red and blue rectangles indicate the two different dykes used for velocity measurements (Modified Yoshida. 2020).

Acknowledgements

This study was supported by the Ministry of Education, Culture, Sports, Science and Technology (MEXT) of Japan, under its The Second Earthquake and Volcano Hazards Observation and Research Program (Earthquake and Volcano Hazard Reduction Research), the Visitors' Joint-Use Program, Marine Core Research Institute, Kochi University (19A032, 19B029, 20A066, 20B058, 22A052, 22B046), and Ritsumeikan University.

References

ICDP, The Thrill to Drill, 2019. https://www.icdp-online.org/fileadmin/icdp/media/doc/The_Thrill_To_Drill_2018_HR_small.pdf

Ogasawara, H. et al., 2019 status report: Drilling into Seismogenic zones of M2.0–M5.5 Earthquakes in South African Gold Mines (DSeis Project). Proc. 9th Int. Congr. Deep and High Stress Mining, Symposium Series S98, Southern African Institute of Mining and Metallurgy, 375-384, 2019.

Yoshida, S. Drilling, core logging, and in-hole geophysical logging of ICDP DSeis drilling into the M5.5 aftershock zones in a South African gold mine, Ritsumeikan University, Master's thesis, 2020.

Tadokoro, R. High-precision source determination for aftershocks of the M5.5 Orkney earthquake using dense seismic network data from underground pits in a South African gold mine, Ritsumeikan University, Master's thesis, 2020.

OGo14

Introduction of PROTEA
-Drilling project to probe the heart of an earthquake and life in the deep subsurface-

Yasuo Yabe[1], Musa Manzi[2], Alba Gómez-Arias[3], Devan Nisson[4], Julio Castillo[3], Raymond Durrheim[2], Hiroshi Ogasawara[5], Thomas Kieft[6], Scott Perl[4]
[1] *Tohoku University,* [2]*Univ. of the Witwatersrand,* [3] *Univ. of the Free State,* [4] *NASA,* [5] *Ritsumeikan Univ. and* [6] *New Mexico Tech.*

How heterogeneous are the in situ frictional properties of the source fault of an earthquake? How do the in situ stress states vary around the source fault? What geological and hydrothermal processes affect the mineralogy of the source fault? To answer these questions, many drilling projects have made great efforts to reach the source faults. However, most of the projects have only reached the upper margin of source fault in unconsolidated sediments or weathered rock mass far above the seismogenic zones, and few holes have intersected a seismogenic zone; i) the JAGUARS project in a deep mine in South Africa, which intersected the source fault of a Mw2.2 mining-induced earthquake just 8 m from the hypocenter, and ii) the ICDP-DSeis project that drilled three holes (A-C) targeting the aftershock cloud of an M5.5 Orkney earthquake, South Africa, from a 2.9-km-deep mine tunnel just above the aftershock cloud. The first hole of the ICDP-DSeis project (Hole A; 817 m long) deflected from the target but intersected a fissure containing ancient (1.2 Ga), non-meteoric hypersaline brine hosting a microbial ecosystem. The second hole (Hole B; 700 m long) intersected a fracture zone spatially coincident with the aftershock cloud; rock samples of an active, tectonic seismic fault were successfully recovered for the first time in the world. Hole C (96 m long) was sidetracked along Hole B to recover more samples from the fracture zone.
The fracture zone occurs in an altered lamprophyre dike rich in biotite and talc. Differential stresses in the plane normal to the borehole axis were measured by the diametric core deformation analysis (DCDA) and the deformation rate analysis (DRA) methods to elucidate the spatial variations in the stress state. Further, the frictional properties of the fracture zone were investigated by a series of rate-step tests. The results of these measurements and tests were consistent with the observations that there was no coseismic slip on the fault around the DSeis hole intersection, even though the aftershock activity was high. However, they cannot explain the nucleation and propagation of the mainshock rupture on this fault.
The hypocenter of the Orkney earthquake (yellow star in Figure 1a) is ~2000 m away from a drilling site and slightly farther than the maximum drilling range (1800 m). However, its nucleation zone may extend within the drilling range, as the size of the nucleation zone of an M5.5 earthquake is estimated to be 500-600 m. Within the 1800-m drilling range, there are bright spots (blue stars in Figure 1a) which radiated large amplitude phases, strong motion generation areas (SMGAs, blue ellipses in Figure 1a and a blue line in Figure 1b), and the upper margin of a large slip area (LSA, >70 mm, yellow ellipses in Figure 1a and a yellow line in Figure 1b). Therefore, we are planning a new drilling project, PROTEA, to investigate the frictional properties, stress state, and mineralogy at the heart of the earthquake. In addition, we drill new holes (tens of meters long) intersecting the fissure brine to survey the ecosystems where microorganisms thrive under hypersaline and oligotrophic conditions. Further, we test the hypothesis that seismicity may stimulate microbial activities through H_2 emissions associated with the failure of rock mass.
We will carry out active and passive seismic surveys of the source area of the Orkney earthquake by installing fiber optic and nodal seismometers along the tunnel at 2.9 km depth on which the PROTEA drilling site is established. The fiber optic will also be installed in the PROTEA long-hole and DSeis Hole B. Simultaneous and synchronized seismic data will be recorded both inside the boreholes using DAS (helical wound fiber optic cable) and along the mining tunnel using co-located DAS and nodal recorders (3C sensors). A 500-kg weight-drop will be used as the seismic source for the active seismic survey. As a GPS-time transmitter is used for both time-tagging of the shots and seismic data, this survey will provide a fine structure of the Kaapvaal craton. The Kaapvaal craton was juxtaposed with the East Antarctic craton in East Gondwana. Therefore, comparisons between their crustal structures contribute to a better understanding of the continental break-up processes.
The preliminary proposal of PROTEA was submitted to the ICDP in January 2024. We are preparing to submit the ICDP Workshop proposal. If approved, it would be held in October 2025 to welcome everyone interested in the PROTEA drilling project.

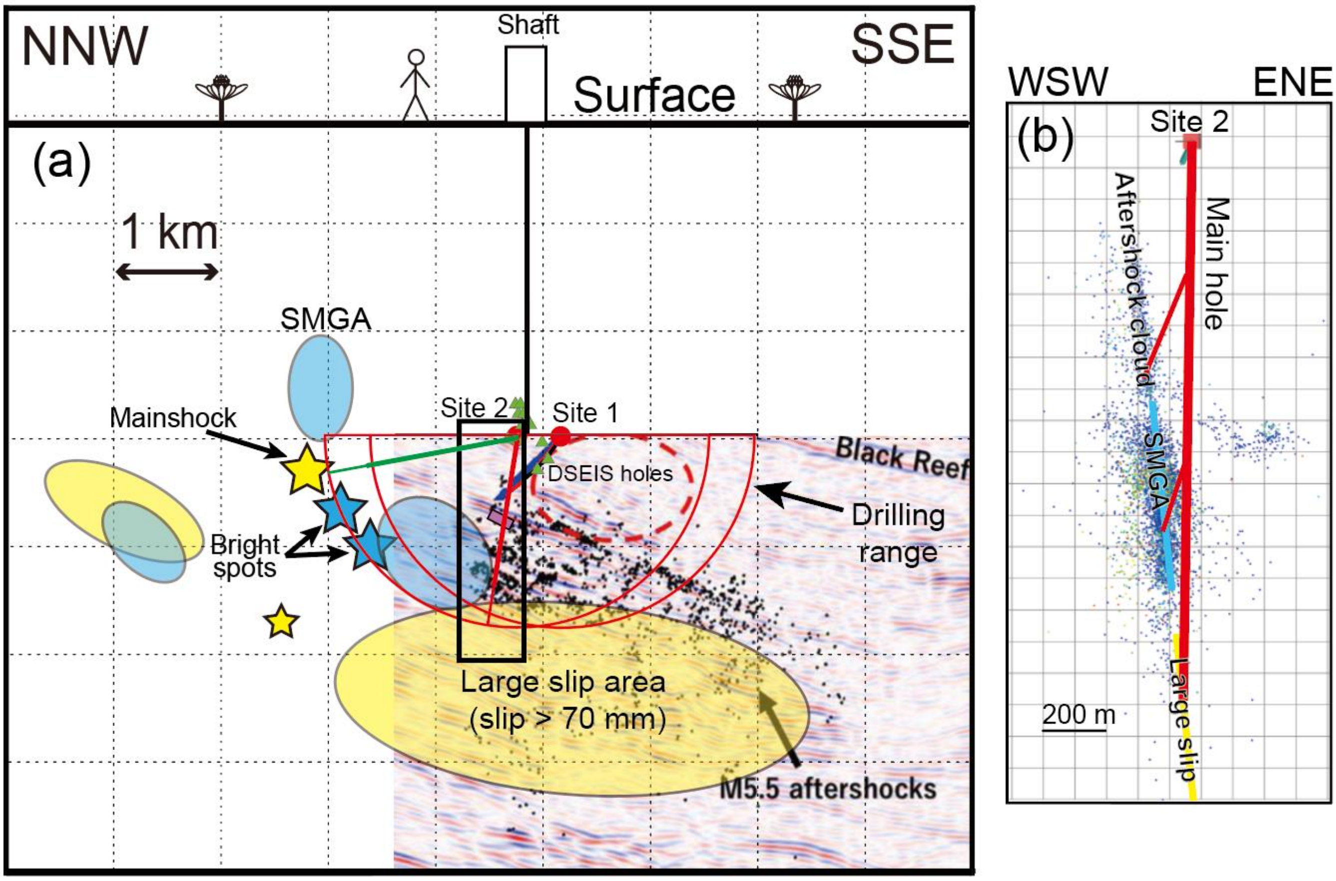

Figure 1. (a) Fault-normal view of LSAs (yellow ellipses) and SMGAs (blue ellipses) relative to the mainshock hypocenter (yellow star). Blue stars are the sources of large amplitude S-waves. Black dots are aftershocks. Colored area in lower right represents a seismic reflection profile. Red semi-circles are 1800-m drilling ranges from Sites 1 and 2. Green and red lines from Site 2 are examples of drilling trajectories targeting the nucleation zone and LAS, respectively. Vertical shaft to 2.9 km depth is shown by a black line. (b) Cross-sectional view of the region enclosed by black square in (a) along the strike of aftershock cloud showing an example of branch drilling (thin red lines) from the main hole (thick red line) to recover samples from SMGA (yellow line) and a lower portion of the aftershock cloud. Yellow line indicates LSA. Colored dots are aftershocks.

OGp1

Contrasting Climate Drivers of East and West Antarctic Mass Change
A mass change coupling in Dronning Maud Land and Amundsen Sea Embayment

Tianyan Shi[1], Jun'ichi Okuno[2], Yoshiya Irie[1]
[1] *Institute for Geothermal Sciences, Kyoto University*
[2]*National Institute of Polar Researchrs*

Since the beginning of the satellite observation era in the early 1990s, most studies have indicated that Antarctica is experiencing and will continue to face long-term mass loss. However, understanding of the climate drivers behind these changes remains insufficient. El Niño-Southern Oscillation (ENSO) and SAM are considered two main drivers.

This study futher explores the long-term mass changes in Antarctica Ice sheet (AIS) and their relationship to large-scale climate indices through correlation analysis. Using Independent Component Analysis (ICA), we separated the AIS mass changes observed by GRACE/GRACE-FO into statistically independent modes. These modes were then compared with climate indices to investigate the primary driving factors.

Our research clarify the connections between AIS mass changes and global-scale climate indices by clustering. Notably, we found significant differences in how Eastern Antarctica (EA) and Western Antarctica (WA) are influenced by large-scale climate drivers. WA is markedly controlled by the ENSO related modes, while EA shows considerably less influence from global climate patterns.

Furthermore, the results suggest a notable coupling between the Amundsen Sea Embayment (AMS) in WA, an area of intense mass loss, and Dronning Maud Land (DML) in EA, which is the primary region of mass gain. Through a comparison of the elevation and mass changes from satellite observation in these two regions, as shown in Figure 1, we discovered a common periodicity of approximately 10.5 years in residual after removing trend and seasonal changes, which both show very strong correlations (>0.7) with the Solar Flux index. Comparison with Surface Mass Balance (SMB) model results indicates that most of these variations could be explained by the SMB.

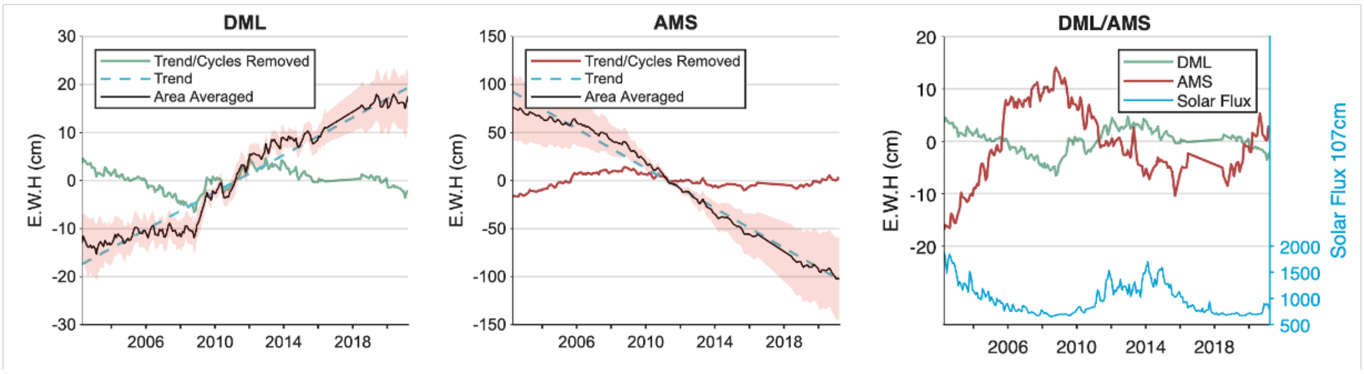

Figure 1. Averaged mass changes in DML and AMS and comparing with Solar Flux index. (Equivalent Water Height: E.W.H.)

Paleomagnetic information from the Lutzow-Holm Complex in East Antarctica

Naoto Ishikawa

Department of Earth System Sciences, School of Sustainable Design, University of Toyama

East Antarctica is one of the key cratons in the formation history of supercontinents during the Earth's history. Tectonic blocks belonging to other cratons of the Gondwana members have been suggested in East Antarctica. After the break-up of the Rodinia supercontinent, East Antarctica craton has been considered to have formed during the formation process of the Gondwana continent at about 550-500 Ma (e.g., Boger, 2011). The Lützow-Holm Complex (LHC) is a metamorphic belt of amphibolite to granulite facies, exposing sporadically along the coast of eastern Dronning Maud Land between 39ºE and 45ºE in East Antarctica. The LHC provides zircon U-Pb ages of Neoproterozoic to early Cambrian (550-520 Ma: e.g., Shiraishi et al., 2003), indicating that metamorphism in the LHC occurred associated with the Pan-African orogeny during the amalgamation of the Gondwana members. Nogi et al. (2013) proposed tectonic blocks in the LHC based on geological structures deduced by magnetic anomaly, gravity anomaly and bedrock topography data, and suggested tectonic movements of the blocks during the Pan-African orogeny. Dunkley at al. (2020) also proposed geological subdivisions in the LHC based on protolith ages of the LHC.

Torsvik et al. (2012) proposed the synthetic apparent polar wonder path (APWP) for Gondwana since 550 Ma, including paleomagnetic poles from Sør Rondane (515Ma) and Victoria Land (500-471 Ma) in East Antarctica. Previous paleomagnetic researches for the LHC reported virtual geomagnetic poles (VGPs) located around the paleopole of 500 Ma in the APWP (e.g., Funaki et al., 1995). The number of paleomagnetic data has been still rare from the LHC as well as East Antarctica. In order to re-examine tectonic movements in East Antarctica during its amalgamation process, paleomagnetic analyses has been performed on samples of the LHC collected at exposed rock areas along the coast of the Lützow-Holm Bay (LHB) and Prince Olav Coast in JARE 35 and 46. Paleomagnetic results from the following nine areas (Figure 1) will be presented in this time: Rundvågshetta (RH: 28 sites), Skallevikshalsen (SVH: 27 sites), Langhovde (LH: 42 sites), Akarui Point (AP: 10 sites), Tenmondai Rock (TR: 11 sites), Niban Rock (NR: 2 sites), Cape Hinode (CHD: 13 sites), Akebono Rock (AR: 10 sites) and Kabuto Rock (KB: 4 sites). Paleomagnetic samples were mainly obtained from gneissic and granitic rocks at those areas, and basaltic dikes of unknown age, intruding to the metamorphic basement, were also collected at CHD and AR. The metamorphic grade of the LHC decreases progressively eastward (Hiroi et al., 1991). Metamorphic rocks at RH in the southern coastal area of the LHB show the highest grade in granulite facies, and SVH and LH are located in the granulite-facies zone. AP belongs to the transitional zone between granulite and amphibolite facies. TR, NR, AR and KB belong to the amphibolite-facies zone. At CHD, metamorphic rocks of granulite facies exist, while amphibolite-facies metamorphic rocks are exposed in the surrounding areas (Hiroi et al., 2006). U-Pb zircon ages of about 1.0 Ga has been reported from the metamorphic rocks, while there is no evidence for ~500 Ma event in the zircons from the rocks (e.g., Shiraishi et al., 2003). CHD has been regarded as an extraneous block in the LHC (Shiraishi et al., 1994)

Progressive thermal demagnetization analyses provided stable remanent magnetic components carried by magnetite, which were isolated in high temperature demagnetization levels generally between about 500ºC and 580ºC. The stable components were shown as straight lines of the demagnetization curves decaying toward the origin of the vector end point diagram. Directions of the components were estimated by applying the principal component analysis to liner trends consisting of more than four demagnetization steps in the demagnetization curves anchored to the origin of the diagram. Estimated directions with maximum angular deviation of 5º or less were used for the further consideration. Site mean directions of the components with radius of 95% confidence circle (alpha-95) smaller than 30º were obtained form 24 sites at RH, 11 sites at SVH, 19 sites at LH, 6 sites at AP, 5 sites at TR, 5 sites at CHD, 1 site at AR and 1 site at KR. The site mean directions were regarded as the directions of characteristic remanent magnetic components (ChRMs) from those areas. The directions of the ChRMs showed normal magnetic polarity except for that from KB, which had reversed polarity and was approximately antipodal to those from other areas.

VGPs calculated from the site means of gneissic and granitic rocks were well grouped at RH, SVH, LH, AP and TR, and an area- mean direction of VGPs from each area has a smaller value of alpha-95 than 15º. As shown in Figure 1, the mean VGPs of those areas were plotted close to a paleomagnetic pols of SR (515 Ma) and the paleopoles of 520-510 Ma in the APWP of Gondwana (Torsvik et al., 2012). According to a zircon U-Pb age (521 Ma: Shiraishi et al., 1994) and biotite K-Ar ages of gneiss and pegmatite in RH (500 Ma, 516 Ma: Fraser and McDougall, 1995) and the distributions of unblocking temperatures for the ChRMs, it is implied that the ChRMs from gneissic and granitic rocks of the LHC at those areas might have been acquired at about 510 Ma in the cooling process from the peak metamorphic stage in the LHC associated with the formation of East Antarctica. It may be suggested that no significant differential tectonic movements have undergone between the subdivided blocks in the LHC since about 510 Ma.

VGPs from CHD appear to be scattered relative to other areas of the LHC (Figure 3). VGPs from gneiss and basaltic sill are plotted near the paleopoles of 530 and 520 Ma in the APWP. A VGP from granitic rocks is located close to the mean VGPs of the LHC at other areas. VGPs from basaltic dikes at HD (2 sites) and AR (1 site) seem to be grouped, and a mean VGP of the three sites is close to the paleopole of 500 Ma in the APWP. Fraser and McDougall (1995) reported K-Ar ages (hornblende, biotite) of 526 and 480 Ma from gneiss and pegmatite. It might have been implied that the ChRMs at CHD were acquired between 530 Ma and 500 Ma, and that the relative position of CHD to other areas of the LHC has not been changed significantly since 530-500 Ma.

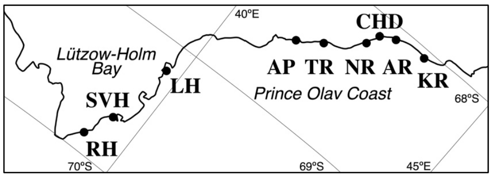

Figure 1. Paleomagnetic sampling areas.

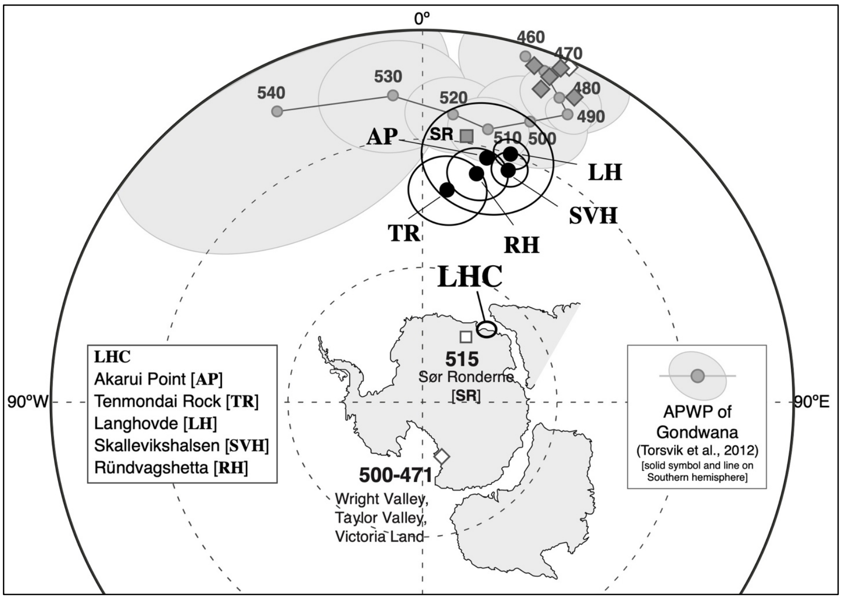

Figure 2. Mean VGPs of gneissic and granitic rocks at 5 areas of the LHC. Solid (open) symbol on the southern (northern) hemisphere.

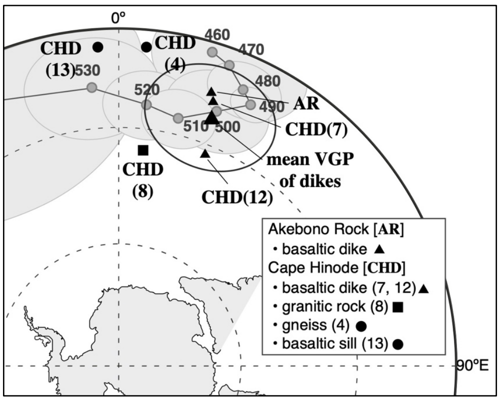

Figure 3. VGPs from Cape Hinode and Akebono Rock.

References

Boger, S.D., Antarctica - Before and after Gondwana, Gondwana Research, 19, 335–371, 2011.

Dunkley J., T. Hokada, K. Shiraishi, Y. Hiroi, Y. Nogi and Y. Motoyoshi, Geological subdivision of the Lützow–Holm Complex in East Antarctica: From the Neoarchean to the Neoproterozoic, Polar Science, 26, https://doi.org/10.1016/j.polar.2020.1006062020, 2020.

Fraser G.F. and I. McDougall, K/Ar and $^{40}Ar/^{39}Ar$ mineral ages across the Lützow-Holm Complex, East Antarctica, Proceedings of the NIPR Symposium on Antarctic Geosciences, 8, 137-159, 1995.

Funaki M., P. Wasilewski and N. Ishikawa, A paleomagnetic study of the west coast region in the Lützow-Holm Bay, The 15th Symposium on Antarctic Geoscience Program and Abstracts, NIPR, 53-54, 1995.

Hiroi, Y., K. Shiraishi, Y. Motoyoshi, Late Proterozoic paired metamorphic complexes in East Antarctica, with special reference to the tectonic significance of ultramafic rocks. In: Thomson, M.R.A., Crame, J.A., Thomson, J.W. (Eds.), Geological Evolution of Antarctica. Cambridge University Press, pp. 83–87, 1991.

Hiroi, Y., Y. Motoyoshi, M. Satish-Kumar, S. Kagashima, Y. Suda and N. Ishikawa, Grunulites from Cape Hinode in the amphibolite-fasies eastern part of Prince Olav Coast, East Antarctica: New evidence for allochthonous block in the Lützow-Holm Complex, Polar Geosciece 19, 89-108, 2006.

Nogi, Y., W. Jokat, K. Kitada and D. Steinhage, 2013. Geological structures inferred from airborne geophysical surveys around Lützow-Holm Bay, East Antarctica, Precambrian Research, 234, 279–287, 2013.

Shiraishi, K., D. J. Ellis, Y. Hiroi, C.M. Fanning, Y. Motoyoshi and Y. Nakai, 1994. Cambrian orogenic belt in East Antarctica and Sri Lanka: Implication s for Gondwana assembly. Journal of Geology, 102, 47–65.

Shiraishi, K., T. Hokada, C.M. Fanning, K. Misawa and Y. Motoyoshi, Timing of thermal events in eastern Dronning Maud Land, east Antarctica. Polar Geosci. 16, 76–99, 2003.

Torsvik T.H., R. Van der Voo, U. Preeden, C.M. Niocaill, B. Steinberger, P.V. Doubrovine, D.J.J. van Hinsbergen, M. Domeier, C. Gaina, E. Tohver, J.G. Meert, P.J.A. McCausland and L.R.M. Cocks, Phanerozoic polar wander, palaeogeography and dynamics, Earth-Science Reviews 114, 325–368, 2012.

OGp3

Understanding Large-Scale Retreat Mechanisms of the Antarctic Ice Sheet through Seamless Sea-Land Geological Drilling

Yusuke Suganuma[1,2], Osamu Seki[3], Yoshimi Kubota[4], Kazuya Kusahara[5], Takeshige Ishiwa[1,2], Atsuko Amano[6], Kota Katsuki[7], Takashi Obase[5]

[1]National institute of Polar Research, 10-3, Midori-cho, Tachikawa, 190-8518, Japan
[2]The Graduate University for Advanced Studies (SOKENDAI), Japan
[3]Institute of Low Temperature Science, Hokkaido University, Sapporo, Japan
[4]National Museum of Nature and Science, Tsukuba, Japan
[5]Japan Agency for Marine-Earth Science and Technology, Yokohama, Japan
[6]Geological Survey of Japan, The National Institute of Advanced Industrial Science and Technology, Tsukuba, Japan
[7]Estuary Research Center, Shimane University, Matsue, Japan

The rapid melting of the Antarctic Ice Sheet (AIS) and the resulting sea-level rise are significant concerns for global climate stability. However, the mechanisms driving major melt events during past warmer periods—key to accurate climate change predictions—remain not fully understood. To address these uncertainties, we have initiated a new project that will conduct comprehensive "sea-land seamless geological drilling" along the Antarctic coast. By utilizing advanced analytical methods on samples dating back to the last glacial period (approximately 20,000 years ago), we aim to reconstruct past climate and ocean conditions and to uncover significant melt processes. Various modeling techniques are also being applied to identify the triggers and conditions that lead to ice sheet melting. This integrated approach will enhance our understanding of AIS melting mechanisms and improve climate change projections. In this presentation, we will discuss the recent outcomes of the project and provide an overview of plans for the next five years.

OGp4

Report on the geological field survey in the regions of Lützow-Holm Bay, Prince Olav Coast and Enderby Land, 2023-2024 (JARE 65)

Tomokazu Hokada[1,2], Tatsuro Adachi[3], Yuki Mori[4] and Sreehari Lakshmanan[5]
[1] *National Institute of Polar Research*
[2] *Polar Science Program, Graduate Institute for Advanced Studies, SOKENDAI*
[3] *Kyushu University*
[4] *Japan Synchrotron Radiation Research Institute*
[5] *Shimane Univrsity*

The team of the geological field project (AP1004) of the Japanese Antarctic Research Expedition (JARE) conducted the geological field survey in the regions of Lützow-Holm Bay, Prince Olav Coast and Enderby Land in the 2023-2024 season (JARE-65). This part of the Antarctic continent comprises of deep crustal high-grade metamorphic and plutonic rocks that recorded the geologic history from early Archaean through Proterozoic to earliest Paleozoic over 3 billion years. For these perspecties, the area is considered by many geologiststs as an ideal field for investigating long Earth history and deep crustal processes. Following the temporal geologic summary by Shiraishi et al. (2008), significant scientific advance has been made especially by the JARE's geology teams. In this presentation, we will review the recent update of the basement geology of eastern Dronning Maud Land and Enderby Land (e.g., Dunkley et al., 2020; Hokada et al., 2024), and report the geological field survey by JARE 65 (2023-2024).

References

Dunkley, D.J., Hokada, T., Shiraishi, K., Hiroi, Y., Nogi, Y., Motoyoshi, Y., Geological subdivision of the Lützow–Holm Complex in East Antarctica: from the Neoarchean to the Neoproterozoic. Polar Science, 26, 100606, 2020.

Hokada, T., Satish-Kumar, M., Kawakami, T., Recent advances in mineralogy, petrology, geochemistry, and geochronology in East Antarctica. Journal of Mineralogical and Petrological Sciences, 119, S002, 2024.

Shiraishi, K., Dunkley, D.J., Hokada, T., Fanning, C.M., Kagami, H., Hamamoto, T., Geochronological constraints on the Late Proterozoic to Cambrian crustal evolution of eastern Dronning Maud Land, East Antarctica: a synthesis of SHRIMP U-Pb age and Nd model age data. In: Satish-Kumar, M. et al. (Eds.), Geodynamic Evolution of East Antarctica: A Key to the East-West Gondwana Connection. Geological Society, London, Special Publication, 308, 21-67, 2008.

OGp5

Growth history of garnet in pelitic gneisses from the highest-grade Ryoke metamorphic complex in Yanai area, SW Japan

Risa Hayashi[1], Takeshi Ikeda[1], Yoshihiro Nakamura[2] and Yumiko Harigane[2]
[1]*Kyushu University*
[2]*Geological Survey of Japan, National Institute of Advanced Industrial Science*

Chemical zoning of garnet and its grain size distribution would provide information on P-T evolution and history of garnet growth during metamorphism. These features have been investigated based on an implicit assumption that the garnet grain is composed of a single crystal. This study evaluates the validity of this assumption using an electron backscatter diffraction (EBSD) for garnet grains in a pelitic gneiss of the Ryoke metamorphic complex in Yanai area, SW Japan.

The studied gneisses were collected from the garnet-cordierite zone, the highest-grade area of the Ryoke metamorphism. The paragenesis and P-T conditions suggest that the garnet in the eastern part nucleated by a continuous reaction (1), Sil + Bt + Qtz = Grt + Kfs + L, followed by a dehydration melting reaction (2), Sil + Bt + Qtz = Grt + Crd + Kfs + L. In contrast, garnet in the western part nucleated by the reaction (2). The garnet from the both parts further grew by a continuous reaction (3), Bt + Crd = Grt + Kfs +L. All the grains show depletion in the Mg content at their periphery, which is indicative of retrograde modification. Some grains experienced collision as judged from the presence of multiple peaks of the Ca content in a grain. Two stages of the collision can be distinguished. They are before and after the retrograde modification, based on the absence or presence of Mg depletion along the collision boundary. The collision took place only after the retrograde modification in the eastern part in contrast to the western part where it took place both before and after the retrograde modification. The eastern grains contain several layers of high P content, whereas the western grains contain only one layer.

The EBSD reveals that 4 of 41 grains in the east and 39 of 574 grains in the west are polycrystalline. In one sample in the west, 34 of 551 grains of garnet are polycrystalline most of which are composed of two crystals. Each grain of <0.02 mm in diameter consists of single crystal. The fraction of the polycrystalline grains increase with increasing grain size. The polycrystalline grains of <0.1 mm are composed of mainly of two crystals with various size, whereas those of >0.1 mm comprise a crystal of <0.04 mm and the another crystal occupying the rest.

The phosphorus has a low diffusion coefficient and is unlike to diffuse at high temperatures, so it is thought to record the growth process of garnet during prograde metamorphism. The multiple layers of phosphorus in the easten garnet implies that they nucleated prior to the western grains and experienced more growth processes. This suggests that the eastern grains nucleated during a continuous reaction (1), while the western grains nucleated during the subsequent dehydration melting reaction (2).

The absence of polycrystalline grains of <0.02 mm suggests that the venue of nucleation spanned more that 0.02mm: the crystals did not collide untile they grew to 0.02mm. The crystals of <0.1 mm collided with nearby grains with various size. This implies that small garnet crystals formed cluster. In contrast, the crystals of >0.1 mm collided with small crystal. This suggests that there were no coarse crystals around the coarse crystal, which is indicative of sparse occurrence of coarse crystals. These spatial occurrence of garnet before collision mimics the present occurrence of isolated coarse grains in leucocratic layers and fine grains in clusters in melanocratic layers. The dehydration melting reaction would enhance the lithological layering such that the melt produced by the reaction was segregated to form leucocratic layers. Such heterogeneity in the rocks also influenced the growth mechanism of garnet.

OGp6

Multiple adakitic magma genesis in the western Lützow-Holm Complex, East Antarctica

Nobuhiko Nakano[1], Sotaro Baba[2], Shin-ichi Kagashima[3] and Fransiska, A.C. Wahyuandari[4]

[1] *Division of Earth Sciences, Faculty of Social and Cultural Studies, Kyushu University*

[2] *Department of Science Education, University of the Ryukyus*

[3] *Department of Earth Sciences, Yamagata University*

[4] *Graduate School of Integrated Sciences for Global Society, Kyushu University*

The Lützow-Holm Complex, situated within past orogeny, is a critical terrane in understanding the evolution of East Gondwana. In order to understand the collisional orogeny that occurred during the formation of Gondwana, it is necessary to determine which continents were present in the orogenic belt. This study focuses on investigating the protolith of felsic gneisses in the western Lützow-Holm Complex, particularly in the southern Lützow-Holm Bay area, which includes the Berrnabbane, Rundvågshetta, Strandnibba, and Instekleppane exposures.

The mineral assemblage of felsic gneisses varies between different rock exposures. In Berrnabbane, the main type of felsic gneiss is hornblende–biotite gneiss, while in the southern part of Instekleppane, garnet–biotite gneiss is common. Orthopyroxene–clinopyroxene±hornblende±biotite gneisses are widely observed in the Strandnibba and in the central to southern Rundvågshetta. Leucocratic gneisses are occasionally found alongside the felsic gneisses in most exposures, and garnet-free mafic granulites are often observed as lenses or blocks within the felsic gneisses. Pyroxenite blocks can be found in Berrnabbane and Strandnibba.

The whole-rock compositions of felsic gneisses and leucocratic gneisses vary, with SiO_2 ranging from 53–76 wt%, K_2O from 0.8–7.3 wt%, and Mg# from 29–60. Most of these rocks exhibit adakitic compositions, characterized by high-Sr/Y and -La/Yb ratios. The mafic granulites found within the felsic gneisses are typically high in Mg (Mg#=60–73), and some samples exhibit low SiO_2/Al_2O_3 ratios, reminiscent of komatiitic basalt. Pyroxenite blocks display extremely high Mg, Cr, and Ni (Mg#≈80, Cr≈3000 ppm; Ni=600–900 ppm), resembling mantle peridotite.

Zircon U–Pb dating indicates that felsic gneisses have upper intercept ages around 2.5 Ga. Their εHf values concentrate ranging from +2 to +8, which are similar to the values of the depleted MORM source mantle. The chemical and isotopic characteristics, as well as the field relations between the felsic gneiss and mafic and ultramafic rocks, suggest that the adakitic protolith was formed through the partial melting of basaltic oceanic crust and the interaction between the slab melt and mantle wedge peridotite around 2.5 Ga. In contrast, oscillatory-zoned zircon in leucocratic gneiss with adakitic composition in Strandnibba has been dated to have a mean age of 570 ± 4 Ma. Some zircon grains exhibit a replaced rim indicating an age of around 530 Ma. The oscillatory-zoned zircon demonstrates bimodal extremely negative εHf values of -21 to -23 and -27 to -30. The former value corresponds to a Hf model age similar to felsic gneisses (2.6–2.9 Ga), suggesting that the protolith of leucocratic gneiss formed from the partial melting of a 2.5 Ga old adakitic protolith in an earlier stage of collision orogeny. Subsequently, both rocks underwent metamorphism during a later event at 550–530 Ma. The lower εHf values in leucocratic gneiss correspond to model ages of 3.2–3.4 Ga, which might indicate the presence of a former continent older than 2.5 Ga

P-T-fluid evolution and oxygen fugacity variations interpreted from calc-silicate granulite of Rundvågshetta, Lützow-Holm Complex, East Antarctica

Koyomi Abe[1], J.A.D. Connolly[2], Tomokazu Hokada[3] and M. Satish-Kumar[1]
[1]*Department of Geology, Faculty of Science, Niigata University, Niigata 950–2181, Japan*
[2] *ETH Zurich, Zurich, Switzerland*
[3] *National Institute of Polar Research, 10-3 Midori-cho, Tachikawa, Tokyo 190-8518, Japan*

Calc-silicate rocks provide a unique oportunity not only to understand the *P-T*-fluid evoluiton in high-grade terranes, but also has the potential to reveal the oxygen fugacity conditions in orogenic belts (e.g. Satish-Kumar et al 2006; Dasgupta and Pal, 2005). The Lützow-Holm Complex (LHC) of East Antarctica is known for its occurrence of high- to ultrahigh-temperature metamorphic rocks. LHC is characterized by an increase in metamorphic grade from amphibolite facies in the northeast to granulite facies in the southwest region, a clockwise *P-T* path and a thermal maximum at Rundvågshetta (Motoyoshi and Ishikawa, 1997; Yoshimura et al., 2008). The major rock types of Rundvågshetta are Cpx-Opx-Hbl gneiss, Grt-Bt gneiss and Grt-Sil gneiss. Minor rock types of Crd-bearing Grt-Opx granulite and Grt-Opx-Sil granulite occur as lenses and layers within the Grt-Bt gneiss and Grt-Sil gneiss. In the southern and central area of this region, the compositional layers are parallel to lithological boundary which strike WNW-ESE in general and dip to the south at 50-70°. On the other hand, in the northern area, the strike directions are disturbed due to antiform dipping 10-30° (Motoyoshi and Ishikawa, 1997). Peak metamorphism occured between 520 and 550 Ma (Shiraishi et al., 1994), with the condition of 1000 °C at 11 kbar. In the central region of Rundvågshetta, a calc-silicate granulite rock within a pyroxene gneiss was reported by the JARE-46 (Satish-Kumar et al., 2006). Although calc-silicate rocks provide us with useful information to deduce the metamorphic evolution of this region, limited work has been done. Therefore, this study report detail information about the calc-silicate rock from Rundvågshetta and construct *P-T* pseudosections to reconsider a *P-T* evolution of the region.

The calc-silicate rock shows a mineralogical zoning, with a rim, intermediate and core zone. The rim zone has a mineral assemblage of Plg + Qtz + Cpx + Scp set in a granular texture. The intermediate zone consists of Plg + Grt + Cpx + Scp ± Qtz. The core of the calc-silicate block has mineral assemblage of Grt + Scp + Qtz ± Cpx, and the garnet grains are porphyroblastic in texture. All zones contain titanite as an accessory mineral. Garnet has a composition of grossular-andradite solid solution with minor other components. Porphyroblastic garnet is nearly pure grossular, on the other hand, garnet which form corona surrounding other minerals show wide range of chemical composition of almost pure grossular to andradite component up 50 %, resulting from a local increase in hydrous fluid activity during retrogression (Satish-Kumar et al. 2006). In order to discuss the *P-T* evolution and fluid composition in more detail, *P-T* pseudosections in the CaO-FeO-Al_2O_3-SiO_2-H_2O-CO_2-Fe_2O_3 system were constructed with the software Perple_X_7.1.6 (Connolly, 2005) based on the result of bulk rock chemical composition obtained from XRF analysis. The *P-T* pseudosections show that peak metamorphic condition, which has a range of 800 °C to UHT condition. Garnet is stable in a wide range of *P-T* condition, on the other hand, plagioclase disappears on the high temperature side. Also, the T-$X(Fe_2O_3)$ pseudosections constructed accordingly show that Cpx become unstable in the range of high $X(Fe_2O_3)$. According to Dasgupta et al. (2005), oxygen fugacity is the crucial variable controlling garnet composition in calc-silicate rocks. This study suggest that the garnet composition may change to grossular-rich at lower $X(Fe_2O_3)$ and andradite-rich at higher $X(Fe_2O_3)$.

References

Motoyoshi, Y. and Ishikawa, M., 1997. Metamorphic and structural evolution of granulites from Rundvågshetta, Lützow-Holm Bay, East Antarctica. The Antarctic Region: Geological Evolution and Processes, ed. by C.A. Ricci. Siena, Terra Antarct. Publ., 65-72.

Yoshimura, Y., Motoyoshi, Y. and Miyamoto, T., 2008. Sapphirine 1 quartz association in garnet: implication for ultrahigh-temperature metamorphism at Rundvågshetta, Lützow-Holm Complex, East Antarctica. Geological Society Special Publication 308.

Shiraishi, K., Ellis, D. J., Hiroi, Y., Fanning, C. M., Motoyoshi, Y. and Nakai, Y., 1994. Cambrian orogenic belt in East Antarctica and Sri Lanka: Implications for Gondwana assembly. Journal of Geology, 102, 47–65.

M. Satish-Kumar, Motoyoshi, Y., Suda, Y., Hiroi, Y. and Kagashima, S., 2006. Calc-silicate rocks and marbles from Lützow-Holm Complex, East Antarctica, with special reference to the mineralogy and geochemical characteristics of calc-silicate mega-boudins from Rundvågshetta. Polar Geosci., 37-61.

Connolly J.A.D., 2005. Computation of phase equilibria by linear programming: A tool for geodynamic modeling and its application to subduction zone decarbonation. Earth and Planetary Science Letters 236:524-541.

Dasgupta, S. and Pal, S., 2005. Origin of Grandite Garnet in Calc-Silicate Granulites: Mineral–Fluid Equilibria and Petrogenetic Grids. Journal of Petrology, 46 (5), 1045–1076.

OGp8

Structural Evolution of the Kasumi Rocks, Lützow-Holm Complex: Role of Pegmatites in Shaping Continental Collision Zones in the East Antarctica

Lakshmanan Sreehari[1], Tomokazu Hokada[2], Tatsuro Adachi[3], Yuki Mori[4]
[1]*Shimane University*
[2]*NIPR*
[3]*Kyushu University*
[4]*SPring-8*

The Kasumi Rocks, located approximately 150 km northeast of Syowa Station within the Lützow-Holm Complex in East Antarctica, encompass a prominent outcrop area of ~2 km². The major lithological units include biotite gneiss, pink gneiss, granitic pegmatite, amphibolite, marble, skarn, and minor ultramafic rocks. Field observations indicate that granitic rocks crosscut amphibolites, while marbles and ultramafic rocks occur as enclaves within the granitic units. A significant unit in the Kasumi Rocks is granitic pegmatite containing megacrystic K-feldspar, which appears to intrude parallel to the gneissic foliation. A subsequent generation of granitic pegmatite crosscuts all units, representing the youngest magmatic activity in the region. Previous studies have determined U-Pb zircon ages for the biotite gneiss as 984 ± 6.9 Ma (Tsunogae et al., 2015) and Rb-Sr isochron ages for the granitic pegmatites at 491.2 ± 23.4 Ma (Ajishi et al., 2004). The Kasumi Rocks are situated within the amphibolite facies and are considered part of an volcanic arc unit in a continental collision zone system (Tsunogae et al., 2015).

This study aims to elucidate the structural relationships of the Kasumi Rocks and the role of pegmatites in governing regional-scale structures, based on data obtained during the JARE-65 fieldwork. Structural relations were analyzed through aerial photography, geological mapping, and microstructural observations on oriented thin sections. Three major and three minor deformation events were identified. The major deformation events include diagenesis and initial foliation development (S_0/S_1) in metasedimentary rocks, such as marble, although this foliation has been largely overprinted by subsequent events. S_2 foliation is associated with isoclinal overturned to recumbent F_2 folds, whose axial planes trend NNW-SSE to NW-SE. These F_2 folds are refolded by F_3 upright isoclinal folds, which plunge obliquely to the north or south, with axial planes trending NW-SE to NNW-SSE. Mineral lineations are generally parallel or subparallel to the plunging hinge lines of the F_3 folds, trending N-NE to S-SW. Minor deformation events include an earlier phase of foliation ($S_{(-1)}$) observed exclusively in ultramafic enclaves, which is oblique to the S_0 to S_3 foliations. Additionally, a ductile shear zone with a top-to-the-north sense of movement, ranging from 5 to 90 cm in width, was observed in two locations. The final minor deformation event is characterized by F_4 open folds with N-S trending axial planes, and a ductile shear zone associated with the late stages of pegmatite emplacement. In mesoscopic and microscopic observations biotite is the prominent mineral observed parllel to the foliation planes in all the major deformtion events. Our observations show that only one set of prominent lineation for major events of folding (F_2 and F_3) and same mineral (biotite) aligned parllel to the both foliations (S_2 and S_3). This probably points to a continuous deformation associated with a collision orogeny than separate deformation events.

As illustrated in Figure 1, the geological map of the Kasumi Rocks reveals that pegmatites are a prominent lithological unit, primarily intruding parallel to the S_2 and S_3 foliations, though cross-cutting relationships are occasionally observed. Despite being involved in regional-scale folding events, these pegmatites have remarkably preserved their solid-state fabrics. This observation aligns with the "pegmatite paradox" described by Butler and Trovela (2018), which highlights the unexpected mechanical strength of syn-deformational pegmatites, typically considered weaker during the ductile deformation.

In the Kasumi Rocks, pegmatites demonstrate enhanced mechanical competence, as indicated by the formation of necking and boudinage structures within the biotite gneiss. Detailed analysis reveals that megacryst feldspar within the pegmatites is typically situated near the contact zones with host rocks. Recent studies (e.g., Phelps et al., 2020) suggest that pegmatites crystallizes rapidly, and this rapid crystallization, combined with the positioning of feldspar near contact zones, may have contributed to their preservation of solid-state fabrics and enhanced mechanical strength. Furthermore, leucocratic veins derived from these pegmatites, which are granitic in composition, have intruded surrounding units and deformed as a weaker phase relative to the host rocks. These findings suggest that pegmatites in the Kasumi Rocks play a significant role in controlling the structural architecture of the region. Further research is needed to explore these dynamics in detail.

References

Ajishi, H., Kawano, Y., Kawakami, T., & Ikeda, T. (2004). Geochronological study of post-metamorphic granite from Kasumi Rock, Lutzow-Holm Complex, East Antarctica. Polar geoscience, 17, 35-44.

Butler, R. W., & Torvela, T. (2018). The competition between rates of deformation and solidification in syn-kinematic granitic intrusions: Resolving the pegmatite paradox. Journal of Structural Geology, 117, 1-13.

Phelps, P. R., Lee, C. T. A., & Morton, D. M. (2020). Episodes of fast crystal growth in pegmatites. Nature communications, 11(1), 4986.

Tsunogae, T., Yang, Q. Y., & Santosh, M. (2015). Early Neoproterozoic arc magmatism in the Lützow-Holm Complex, East Antarctica: Petrology, geochemistry, zircon U–Pb geochronology and Lu–Hf isotopes and tectonic implications. Precambrian Research, 266, 467-489.

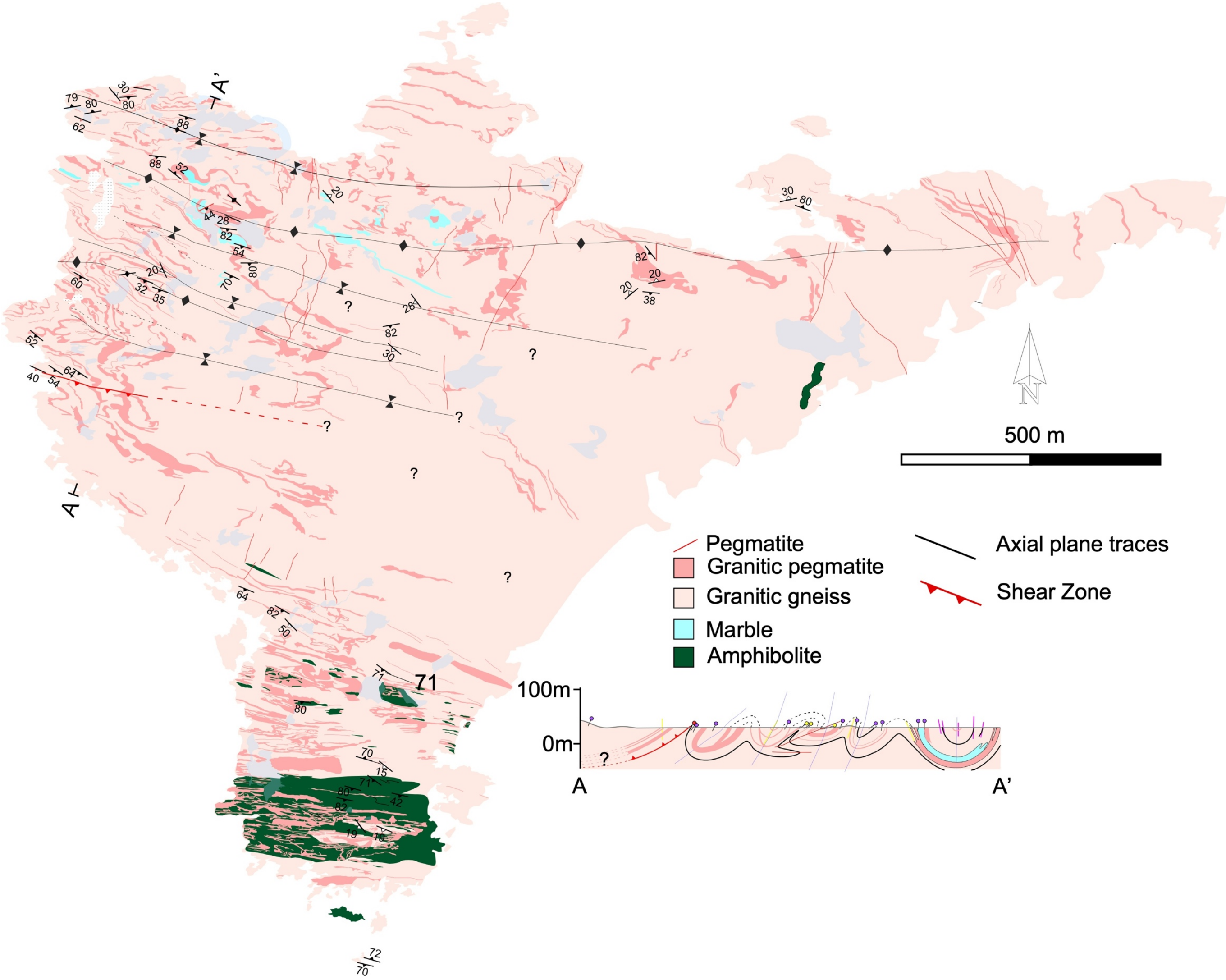

Figure 1: Geological map of the Kasumi Rocks. Pegmatite folded along with granitic gneiss are visible in regional-scale.

Preliminary report of REE compositions of zircon and garnet in a sillimanite-biotite-garnet gneiss from Mefjell, Sør Rondane Mountains, East Antarctica

Miku NAKANO[1], Fumiko HIGASHINO[1], Tetsuo KAWAKAMI[1], Shumpei KUDO[1], Tatsuro ADACHI[2], Sota NIKI[3], Masaoki UNO[4], Cheolwoo KIM[1] and Takafumi HIRATA[5]

[1]Kyoto University, [2]Kyushu University, [3]Nagoya University, [4]Tohoku University, [5]The University of Tokyo

The Sør Rondane Mountains (SRM) in eastern Dronning Maud Land, East Antarctica are considered to be located at the crossing point of the East African Orogen at ca. 750-620 Ma, and Kunnga Orogen at ca. 570-530 Ma (Meert, 2003; Satish-Kumer et al., 2013). The SRM are the key area to understand the formation process of Gondwana supercontinent. The SRM are divided into two terranes; the NE terrane which is mainly composed of granulites with clockwise pressure-temperature-time *(P-T-t)* path and the SW terrane composed of granulites and lower-grade metamorphic rocks with counter-clockwise *P-T-t* path (Osanai et al., 2013). The timings of peak and retrograde metamorphism are interpreted to be 650-600 Ma and 590-530 Ma in both terranes using U-Pb dating of separated zircon grains (Osanai et al., 2013). However, recent studies have reported *P-T-t* paths or timings of high-grade metamorphism inconsistent with the tectonic model of Osanai et al. (2013) (e.g., Kawakami et al., 2017; Tsubokawa et al., 2017; Higashino et al., 2023). Recently, a hair-pin-shaped clockwise *P-T-t* path was reported from Mefjell in the central SRM (Tsubokawa at al., 2017), although Mefjell belongs to the SW terrane from which counter-clockwise path is expected (Osanai et al., 2013). Nakano et al. (2023) also reported a hair-pin-shaped clockwise *P-T* path with the peak temperature of 725 °C by applying the Zr-in-rutile geothermometer (Tomkins et al., 2007) to a sillimanite-biotite-garnet gneiss (sample TK2019122301A) from Mefjell. Tsubokawa et al. (2017) reported 700-540 Ma as the timing of peak metamorphism by electron microprobe (EMP) U-Th-Pb dating of matrix monazite. However, they did not take the chemical zoning of monazite into consideration and discuss the equilibrium relationship between garnet and monazite. Nakano et al. (2024) interpreted the timings of garnet-forming metamorphism and retrograde metamorphism in Mefjell to be at ca. 650 Ma and ca. 550 Ma, respectively, through the EMP U-Th-Pb dating of monazite, using Y concentration in monazite (cf, Foster et al., 2000). In addition to monazite, zircon is an appropriate mineral to evaluate the timing of garnet formation. Since garnet prefers heavy rare earth elements (REE) (Rubatto, 2017), it is possible to evaluate the equilibrium relationship between zircon and garnet by using distribution coefficient of REE (D_{REE}) (e.g., Taylor et al., 2017). In order to confirm the equilibrium relationship between zircon and garnet, we conducted U-Pb dating of zircon and measurement of trace elements in zircon and garnet.

The studied sample is a sillimanite-biotite-garnet gneiss TK2019122301A (Nakano et al., 2023, 2024). A garnet porphyroblast has discontinuous chemical zoning in P that diffuses slowly in garnet. Using the P zoning as contemporaneous surfaces, garnet can be divided into P-poor inner core, P-rich outer core, P-poor mantle, and moderately P-bearing rim (Nakano et al., 2023). The M-HREE patterns of the garnet inner core, outer core, mantle and rim are flat to positive (Yb_n/Gd_n = 2.1-27), negative to flat (Yb_n/Gd_n = 0.31-2.7), flat (Yb_n/Gd_n = 1.3-5.1) and negative to flat (Yb_n/Gd_n = 0.11-1.1).

On the other hand, zircon consists of inherited core, metamorphic core, and metamorphic rim. The metamorphic core shows oscillatory zoning under CL images, and includes quartz, sillimanite, K-feldspar, biotite, apatite, and graphite. The metamorphic rim has both bright and dark domains in CL images and includes sillimanite, K-feldspar, and rutile. Both the metamorphic core and rim are divided into two groups; low Yb_n/Gd_n ratio group (Yb_n/Gd_n = 0.27-3.8) and high Yb_n/Gd_n ratio group (Yb_n/Gd_n = 21-52) except for one analysis point. The low Yb_n/Gd_n ratio group gave the weighted-mean ^{238}U-^{206}Pb ages (±2σ) of 637±41 Ma (n=3; MSWD=1.8; Th/U≤0.16) for metamorphic core and 562±8 Ma (n=7; MSWD=1.14; Th/U≤0.02) for the metamorphic rim whereas the high Yb_n/Gd_n ratio group gave the weighted-mean ^{238}U-^{206}Pb ages of 628±27 Ma (n=5; MSWD=4.0; Th/U≤0.02) for the metamorphic core and 567±16 Ma (n=2; MSWD=0.032; Th/U≤0.03) for the metamorphic rim. Since the metamorphic rim of zircon included in the garnet rim shows a ^{238}U-^{206}Pb date of 566±21 Ma (Yb_n/Gd_n=28), garnet rim may postdate 566±21 Ma. In the presentation, we will discuss the equilibrium relationship of garnet and zircon by using array plots by Taylor et al. (2017).

References

Foster, G., Kinny, P., Vance, D., Prince, C., Harris, N., The significance of monazite U–Th–Pb age data in metamorphic assemblages; a combined study of monazite and garnet chronometry, Earth and Planetary Science Letters, 181 (3), 327-340, 2000.

Higashino, F., Kawakami, T., Sakata, S., Hirata, T., Multiple timings of garnet-forming high-grade metamorphism in the Neoproterozoic continental collision zone revealed by petrochronology in the Sør Rondane Mountains, East Antarctica, Gondwana Research, 119, 204-226, 2023.

Kawakami, T., Higashino, F., Skrzypek, E., Satish-Kumar, M., Grantham, G., Tsuchiya, N., Ishikawa, M., Sakata, S., Hirata, T., Prograde infiltration of Cl-rich fluid into the granulitic continental crust from a collision zone in East Antarctica (Perlebandet, Sør Rondane Mountains), Lithos, 274–275, 73–92, 2017.

Meert, J., A synopsis of events related to the assembly of eastern Gondwana, Tectonophysics, 362, 1–40, 2003.

Osanai, Y., Nogi, Y., Baba, S., Nakano, N., Adachi, T., Hokada, T., Toyoshima, T., Owada, M., Satish-Kumar, M., Kamei, A., Kitano, I., Geologic evolution of the Sør Rondane Mountains, East Antarctica: Collision tectonics proposed based on metamorphic processes and magnetic anomalies, Precambrian Research, 234, 8–29, 2013.

Nakano, M., Kawakami, T., Higashino, F., Adachi, T., Uno, M., Clockwise pressure-temperature path from Mefjell, Sør Rondane Mountains East Antarctica, Japan Geoscience Union Meeting 2023 abstract, 2023.

Nakano, M., Higashino, F., Kawakami, T., Adachi, T., Uno, M., Timing of garnet-forming metamorphism constrained by U-Th-Pb electron microprobe dating of monazite in a pelitic gneiss from Mefjell, Sør Rondane Mountains, East Antarctica, Japan Geoscience Union Meeting 2024 abstract, 2024.

Rubatto, D., Zircon: the metamorphic mineral, Reviews in Mineralogy & Geochemistry, 83 (1), 261–295, 2017.

Satish-Kumar, M., Hokada, T., Owada, M., Osanai, Y., Shiraishi, K., Neoproterozoic orogens amalgamating East Gondwana: Did they cross each other?, Precambrian Research, 234, 1–7, 2013.

Taylor, R.J.M., Clark, C., Harley, S.L., Kylander-Clark, A.R.C., Hacker, B.R., Kinny, P.D., Interpreting granulite facies events through rare earth element partitioning arrays, Journal of Metamorphic Geology, 35 (7), 759–775, 2017.

Tomkins, H.S., Powell, R., Ellis, D.J. The pressure dependence of the zirconium-in-rutile thermometer, Journal of Metamorphic Geology, 25, 703-713. 2007.

Tsubokawa, Y., Ishikawa, M., Kawakami, T., Hokada, T., Satish-Kumar, M., Tsuchiya, N., Grantham, G., Pressure–temperature–time path of a metapelite from Mefjell, Sør Rondane Mountains, East Antarctica, Journal of Mineralogical and Petrological Sciences, 112(2), 77-87, 2017.

Occurrence and microstructural characteristics of pseudotachylyte in the Mt. Riiser-Larsen and Mt. Sones, Napier Complex, East Antarctica

Ryo Murayama[1], Lakshmanan Sreehari[1] and Tsuyoshi Toyoshima[2]
[1]*Shimane University*
[2]*Niigata University,*

Pseudotachylytes have been identified at three key locations within the Napier Complex, East Antarctica: Tonagh Island, Mt. Riiser-Larsen, and Mt. Sones. At Tonagh Island, multiple generations of pseudotachylytes formed during the deformation of ultrahigh-temperature (UHT) metamorphic rocks have been extensively studied, focusing on their field distribution and microstructural characteristics (Toyoshima et al., 1999). In contrast, although the presence of pseudotachylytes along the Riiser-Larsen Main Shear Zone (RLMSZ) has been reported (e.g., Ishizuka et al., 1998), detailed structural and microstructural analyses remain limited. The same is true for pseudotachylytes from Mt. Sones. This study aims to clarify the microstructures and mineral assemblages of pseudotachylytes from Mt. Riiser-Larsen and Mt. Sones and to understand their evolutionary history.

Oriented thin sections from the RLMSZ were prepared, and observations using optical microscopy and SEM revealed three distinct types of pseudotachylytes.

Type 1: Mylonitized Pseudotachylyte: These pseudotachylytes, identified using criteria from Nancy et al. (2012), are overprinted by mylonitization. The host rock is granitic mylonite (orthogneiss), consisting of feldspar porphyroclasts and a fine-grained matrix of quartz, biotite, and opaque minerals, with S-C' structures. The veins have a sharp boundary with the host rock and contain feldspar porphyroclasts and quartz islands, with a homogeneous, fine-grained matrix. Asymmetrical structures show a south-to the top sense of movements.

Type 2: Pseudotachylyte with Angular Clasts: Approximately 7 mm wide, these pseudotachylytes are characterized by a sharp boundary with the orthogneiss host rock and a chilled margin of fine-grained quartz, pyroxene, and plagioclase. Angular clasts of pyroxene, plagioclase, and quartz are randomly oriented within a microcrystalline matrix containing pyroxene microlites with acicular, dendritic, and spherulitic textures.

Type 3: Pseudotachylyte with Rounded Clasts: These dark, 1 mm wide veins cross the boundary between orthogneiss and dolerite. The clasts, composed of quartz, plagioclase, pyroxene, amphibole, and ilmenite, are rounded and slightly aligned in the direction of flow structures. The matrix is cryptocrystalline, with only a few microlites of plagioclase, pyroxene, and amphibole.

Pseudotachylytes from Mt. Sones, approximately 5 mm wide and black, penetrate orthogneiss with a sharp boundary (Fig. 1b) and feature injection structures, flow structures, and chilled margins. The clasts within these veins are slightly rounded and include fragments of quartz, plagioclase, and pyroxene. Notably, garnet with cauliflower-like textures (Fig. 1c), likely crystallized from melt, is observed, with size increasing toward the center of the veins. The matrix is cryptocrystalline, containing aligned pyroxene microlites. These garnets and pyroxene are often in mutual contact.

The microstructural analysis reveals distinct differences between the pseudotachylytes from Mt. Riiser-Larsen and Mt. Sones, indicating variations in their formation processes. Type 1 pseuodotachylyte from RLMSZ indicate repititive brittle-ductle deformation exclusively in the region. The garnet-bearing pseudotachylytes from Mt. Sones suggest a lower crustal origin, while those from Mt. Riiser-Larsen likely formed under upper crustal conditions. Additionally, similarities between the Mt. Sones pseudotachylytes and those from Tonagh Island imply that multiple generations of pseudotachylytes formed in the Napier Complex, potentially associated with paleoearthquakes driven by different tectonic events. Further details of these processes will be explored in future research.

Reference

Hideo ISHIZUKA, Masahiro ISHIKAWA, Tomokazu HOKADA and Satoko SUZUKI (1998): GEOLOGY OF THE MT. RIISER-LARSEN AREA OF THE NAPIER COMPLEX, ENDERBY LAND, EAST ANTARCTICA. Polar Geosci., 11, 154-171.

Masahiro ISHIKAWA, Tomokazu HOKADA, Hideo ISHIKAWA, Hideki MIURA, Satoko SUZUKI, Masashi TAKADA and Daniel P. ZWARTZ (2000): Explanatory Text of Geological Map of Mount Riiser-Larsen, Enderby Land, Antarctica. ANTARCTIC GEOLOGICAL MAP SERIES SHEET 37 MOUNT RIISER-LARSEN. NATIONAL INSTITUTE OF POLAR RESEARCH, TOKYO.

Nancy A. Price, Scott E. Johnson, Christopher C. Gerbi, David P. West Jr. (2012): Identifying deformed pseudotachylyte and its influence on the strength and evolution of a crustal shear zone at the base of the seismogenic zone. Tectonophysics 518-521, 63-83.

TOMOKAZU HOKADA, YOICHI MOTOYOSHI, SATOKO SUZUKI, MASAHIRO ISHIKAWA & HIDEO ISHIZUKA (2008): Geodynamic evolution of Mt. Riiser-Larsen, Napier Complex, East Antarctica, with reference to the UHT mineral associations and their reaction relations. Geological Society London, Special Publications 2008, v.308; p253-282.

Tsuyoshi TOYOSHIMA, Yasuhito OSANAI, Masaaki OWADA, Toshiaki TSUNOGAE, Tomokazu HOKADA and Warwick A. CROWE (1999): DEFORMATION OF ULTRAHIGH-TEMPERTURE METAMOROPHIC ROCKS FROM TONAGH ISLAND IN THE NAPIER COMPLEX, EAST ANTARCTICA. Polar Geosci., 12, 29-48.

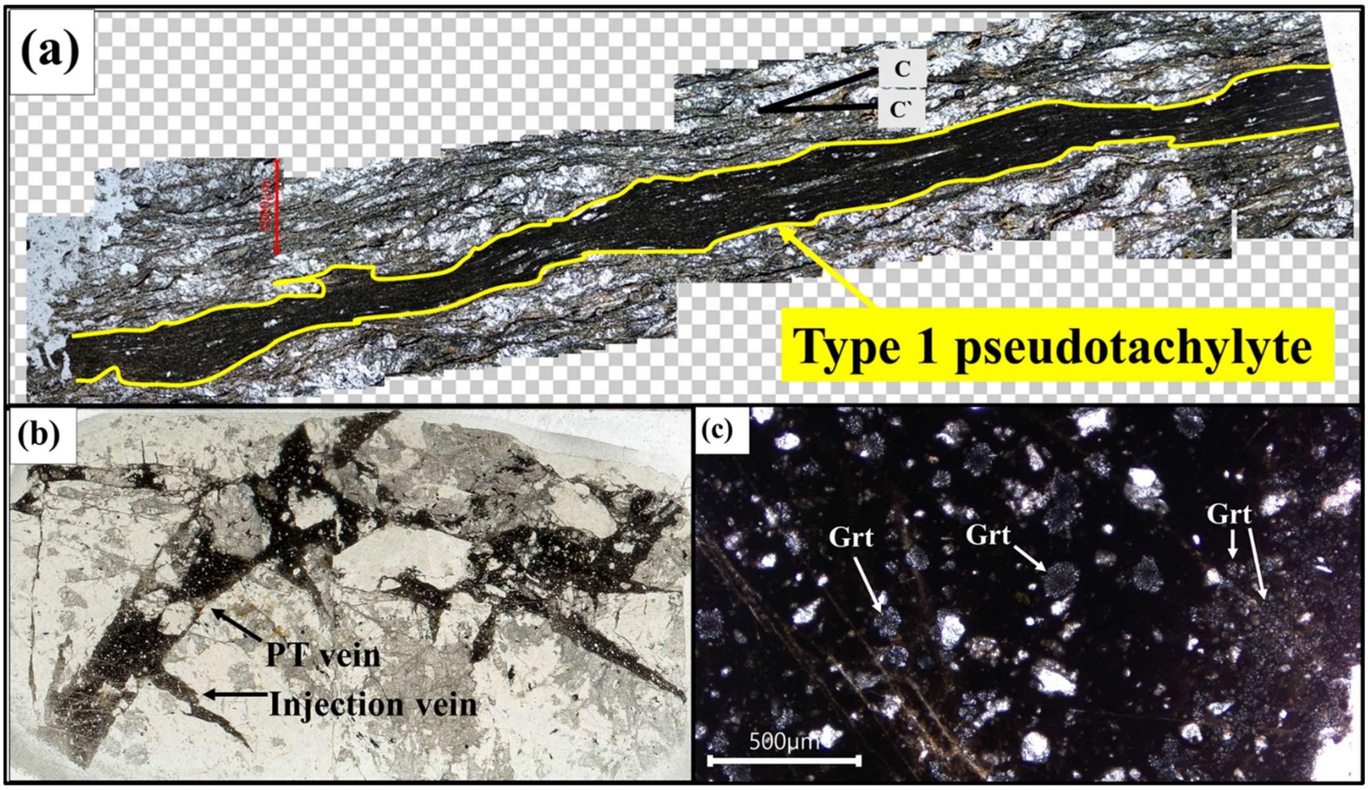

Figure 1 (a). Mylonitized pseudotachylyte from Mt. Riiser-Larsen. Scale bar of red = 1000μm. The area surrounded by the yellow line is Type 1 pseudotachylyte. The two black lines indicate C-C` structure. (b) Thin section of pseudotachylyte (PT) from Mt. Sones. Width of the view 40mm. (c) Cauliflower like garnet in the pseudotachylyte matrix (magnified from figure 1b), note that the size of garnet increases towards the center of the photograph (away from the boundary between pseudotachylyte and host rock).

OGp11

Neoarchean double-sided subduction and continent-continent collision during the assembly of the Kenorland supercontinent: a new tectonic model for the Limpopo Complex in southern Africa

Toshiaki Tsunogae
University of Tsukuba

The Limpopo Complex exposed in South Africa, Zimbabwe, and Botswana has been regarded as a classic example of Neoarchean granulite terranes formed by continent-continent collisional orogeny (e.g., Roering et al., 1995; van Reenen et al., 1987). As the complex is sandwiched by the Zimbabwe Craton to the north and the Kaapvaal Craton to the south, the collision of the two cratons during Neoarchean probably gave rise to the granulite-facies metamorphism of the region (Limpopo orogeny). However, multiple collisional events or diapir-driven granulite formation has also been inferred for the evolution of the complex. The effect of ca. 2.0 Ga thermal event that regionally overprinted the Neoarchean granulites also made the evolutional history of the Limpopo Complex more complicated. A recent review of the geology of southern Africa described that the Limpopo Complex is a Paleoproterozoic orogeny, but this is totally wrong as the Limpopo Complex is cut by the Great Dyke (ca. 2.5 Ga layered intrusion) of the Zimbabwe Craton, so the main high-grade metamorphism of the Limpopo Complex should have been completed by the end of Neoarchean. In order to clarify the timing of the Limpopo orogeny and its tectonics, the author reviewed petrological and geochronological characteristics of different lithological units of the complex, and, together with new monazite age, attempted to explain the tectono-thermal evolution of the Limpopo Complex by double-sided subduction and following continent-continent collision that took place during Neoarchean.

The Limpopo Complex is structurally and lithologically subdivided into three units: the Northern Marginal Zone (NMZ), Central Zone (CZ), and the Southern Marginal Zone (SMZ). The dominant lithologies of the NMZ and the SMZ are felsic to mafic orthogneisses and charnockites with subordinate amount of metabasites (amphibolite and mafic granulite) and metasediments (pelitic granulite and meta-banded iron formation [BIF]). Hf isotopic data of zircons from orthogneisses and charnockites from the NMZ suggest that both the NMZ and the Zimbabwe Craton show similar origin, which support the model that the NMZ and the SMZ are high-grade equivalents of the adjacent cratons (Zimbabwe and Kaapvaal Cratons, respectively). In the SMZ, pelitic granulites are dominant supracrustal lithologies, whereas mafic granulite/amphibolite and meta-BIF are dominant in the NMZ, suggesting that slightly lower crustal level might have been exposed in the NMZ than the SMZ. Field observations of the NMZ indicate that meta-BIFs are dominantly intercalated with metabasites, therefore the rock associations could be remnants of oceanic plate possibly accreted during the convergent tectonics before the final collision. The NMZ orthogneisses and charnockites are calc-alkaline in composition and show magmatic arc-related geochemical characteristics, suggesting that the NMZ corresponds to an active continental margin of the Zimbabwe Craton. Similar geochemical signatures are inferred for the SMZ orthogneisses, therefore the SMZ could also be an active continental margin of the Kaapvaal Craton.

The CZ is different from the marginal zones because of abundant metasedimentary rocks (pelitic granulite, quartzite, meta-BIF, marble) with minor mafic and ultramafic granulites which are not commonly observed in large sedimentary basins. Therefore, the CZ might correspond to trench-filling sediments that accreted before the collision. Therefore, this study infers double-sided subduction of oceanic lithosphere underneath the Zimbabwe and Kaapvaal Cratons, which was followed by the final collision of the two cratons at ca. 2.7 to 2.6 Ga. High-pressure and ultrahigh-temperature (14 kbar and >1000 ºC) metamorphism recorded in the metasediments of the CZ might have formed by post-collisional slab break off and heating of the lower crust by asthenospheric upwelling.

OGp12

Regional Neoproterozoic thermal overprint on the basement rocks in Malawi: New insights from monazite Th-U-Total Pb geochronology of the Mesoproterozoic Irumide Belt

Yuzuki Kikuchi, Toshiaki Tsunogae, Mzee Nkhwachi Nyirongo

Degree Program in Geosciences, University of Tsukuba, Ibaraki 305-8572, Japan

The geology of southern Africa is composed dominantly of Archean cratons and Proterozoic orogenic belts formed by a series of continental collision events. Previous studies indicate that three stages of the orogenic belts are distributed in north-central Malawi (Mozambique, Irumide, Ubendian Belts from south to north; e.g., Fritz et al., 2013), but their boundaries are not clearly defined. In this study, we performed Th-U-total Pb dating of monazites (Kadowaki and Tsunogae, 2020) in high-grade metamorphic rocks in this area for evaluating the relative distribution of the orogenic belts. These samples were collected from the region previously thought to be tectonically part of the Irumide Belt (Late Mesoproterozoic), but four samples show monazite Th-U-Total Pb ages of ca. 1990-1910 Ma, corresponding to the age of the Ubendian Belt (Palaeoproterozoic). As no Mesoproterozoic age corresponding to the Irumide Belt was recorded in these samples, they are considered to be a southern extension of the Ubendian Belt or a block of the Ubendian Belt inside the Irumide Belt. Also, the northeasternmost sample shows Neoproterozoic overprint age of ca. 610 Ma. Such overprint age is also seen in the southern part of the Ubendian Belt in northern Malawi (Wakita 2023Ms), thus the northern part of the Irumide Belt (tectonically) and the southern part of the Ubendian Belt have probably been overprinted by the East African (ca. 650-620 Ma, 580-500 Ma; e.g., Fritz et al., 2013) orogeny.

From the southern part of the Irumide Belt adjacent to the Mozambique Belt, 1100-1050 Ma Mesoproterozoic ages which are consistent with the results of previous studies, have been obtained as well as Neoproterozoic to Ordovician (610-480 Ma) thermal overprinting ages possibly related to the second metamorphism during the East African orogeny. Such prolonged metamorphic evolution could be due to the location of central Malawi around the junction between the two different stages of East African orogeny. Additionally, the distribution of such overprint event in the Irumide Belt is complex, thus the intensity of overprint of the East African orogeny is possibly heterogeneous.

References

Fritz, H., Abdelsalam, M., Ali, K.A., Bingen, B., Collins, A.S., Fowler, A.R., Ghebreab, W., Hauzenberger, C.A., Johnson, P.R., Kusky, T.M., Macey, P., Muhongo, S., Stern, R.J., and Viola, G. (2013) Orogen styles in the East African orogen: a review of the Neoproterozoic to Cambrian tectonic evolution. Journal of African Earth Sciences, 86, 65–106.

Kadowaki, H. and Tsunogae, T. (2020) In-situ EPMA dating of monazites in granulites from collisional orogens in southern India and southern Africa. Earth Evolution Sciences, University of Tsukuba, 14, 3–8.

Wakita Y., 2023MS. Petrology and Geochronology of the Ubendian Belt in northern Malawi. M.Sc. thesis, Degree Program in Geosciences, University of Tsukuba. 93pp

Petrogenesis of garnet + orthopyroxene corona around olivine in metagabbros from the Mozambique Belt in central Malawi

Mirei Kume, Toshiaki Tsunogae, Mzee Nkhwachi Nyirongo
University of Tsukuba

The Precambrian geology of southern Africa is composed of Meso- to Neoarchean cratons and four-stages orogenic belts surrounding them. They are ca. 2.7-2.6 Ga Limpopo Complex, ca. 2.1-1.9 Ga Ubendian-Magondi Belt, ca. 1.1-1.0 Ga Kibaran-Irumide-Namaqualand-Natal Belt, and ca. 600-550 Ma Mozambique-Zambezi-Damara Belt which were probably formed during the amalgamation of supercontinents (Kenorland, Columbia, Rodinia, and Gondwana, respectively). Malawi located in south-central Africa hosts the three Proterozoic orogenic belts (Ubendian, Irumide, and Mozambique Belts from north to south) (e.g., Tsunogae et al., 2021), therefore detailed petrological and geochronological investigations of high-grade metamorphic rocks in Malawi provide important clues for understanding the tectono-thermal evolution of the region. Particularly, the Mozambique Belt in Malawi is located around the junction of two major orogens of Gondwana; the East-African Orogen (650-550 Ma) and the Kuunga Orogen (560-530 Ma), therefore the region might record complex and prolonged thermal history. In this study, we examined petrography, geochemistry, and mineral chemistry of metagabbros that probably intruded into the basement rocks (granitoid gneiss and metasediments) of the Mozambique Belt in central Malawi, and evaluated the petrogenesis of complex reaction textures observed in the metagabbro.

The metagabbro samples were collected from Malomo area, approximately 40 km ESE from Kasungu in central Malawi. They are medium- to coarse-grained and homogeneous rocks composed of olivine, plagioclase, and clinopyroxene as primary magmatic minerals, which is confirmed by ophitic textures observed in medium-grained phases collected from the contact with the host basement rocks. Geochemical characters of the rocks such as higher Th/Yb ratios in the Nb-Th-Yb diagram indicate their magmatic-arc origin. Therefore, the protolith gabbro probably intruded into the Mozambique Belt during high-grade metamorphism. The olivine adjacent to plagioclase is surrounded by reaction coronae composed of orthopyroxene and garnet with minor pargasite, suggesting the progress of the following reaction:

olivine + plagioclase + H_2O => orthopyroxene + garnet + calcic amphibole

It is important to note that previous studies of metagabbro reported corona textures between olivine and plagioclase, but they are dominantly composed of orthopyroxene + calcic amphibole + spinel (e.g., Torres-Rodriguez et al., 2021). There were only a few examples of such corona textures including garnet.

We performed phase equilibrium modeling of the metagabbros in the system Na_2O-CaO-FeO-MgO-Al_2O_3-SiO_2-H_2O-TiO_2 using Perple_X software and obtained a magmatic crystallization temperature of the protolith of the metagabbro as >1200 °C at 7 kbar. The corona assemblage including orthopyroxene, garnet, and calcic amphibole were stable at about 700 °C, which is consistent with the results of garnet-hornblende geothermometry of mafic granulite (730-735 °C at 7 kbar) from an adjacent locality. The results of this study suggest that the gabbro intruded into the middle- to lower-crustal level during the peak (amphibolite facies) metamorphism, and subsequently cooled quickly and formed the corona texture.

References

Torres-Rodriguez, N., Barnes, S.J., Taranovic, V., Pearce, M.A., Verrall, M., Schoneveld, L.E., 2021. Reaction coronas at olivine–plagioclase contacts in host rocks from the Nova–Bollinger Ni–Cu–Co Deposit, Albany–Fraser Orogen, Western Australia: Evidence of a magmatic to metamorphic continuum. Journal of Petrology, 62, 1–24.

Tsunogae, T., Uthup, S., Nyirongo, M.W., Takahashi, K., Rahman, Md.S., Liu, Q., Takamura, Y., Tsutsumi, T., 2021. Neoproterozoic crustal growth in Southern Malawi: New insights from petrology, geochemistry, and U–Pb zircon geochronology, and implications for the Kalahari Craton–Congo Craton amalgamation. Precambrian Research 352, Article 106007, p1-20.

OGp14

Attractive Himalayan Geology – Highlites of the 12th Student Himalayan Field Exercise Tour in March 2024.

Yoshida, M. [1, 2], Sakai, T.[3], Sigdel, A.[2], Silwal, C.B.[2], Arita, K.[4], Upreti, B.N.[5]

[1] Gondwana Institute for Geology and Environment, Hashimoto, [2] Department of Geology, Tri-Chandra Campus, Tribhuvan University, Kathmandu, [3] Faculty of Multidisciprenary Science, Shimane University, Matsue, [4] Hokkaido University Museum, Sapporo, [5]Nepal Academy of Science and Technology, Kathmandu

Abstract

The Himalaya is one of the largest and youngest mountain range on the earth. Reflecting the collisional tectonics of Indian and Eurasian plates, the Himalaya exhibits a clear zonal geologic constitutions. Five geotectonic zones ranging in age from the Proterozoic to the Quaternary are arranged parallel to the mountain range, all zones being bounded by large north-dipping faults, which are mostly thrust. A large uplifting rate of 5 mm/y is still continuing today and resulting to form deep valleys and steep mountain slopes where slope collapse, landslide and river flood often take place. The Himalaya is the living museum for people studying geoscience and natural hazards.

The N-S traverse of the Himalaya along the route connecting the Kaligandaki and Tinau valleys in west-central Nepal is the best geo-excursion course that discloses a full view of the Himalayan Orogen (Yoshida and Ulak, 2017). We have been conducting the Japan-Nepal Student Himalayan Exercise Tour (SHET) every year since 2012 (SHET-HP, 2024, Yoshida and Student Himalayan Field Exercise Project, 2023, Yoshida et al., 2019) and so far 12 field tours under the program were successfully conducted along the above course, and preparation for the 13th tour in next March is under the progress.

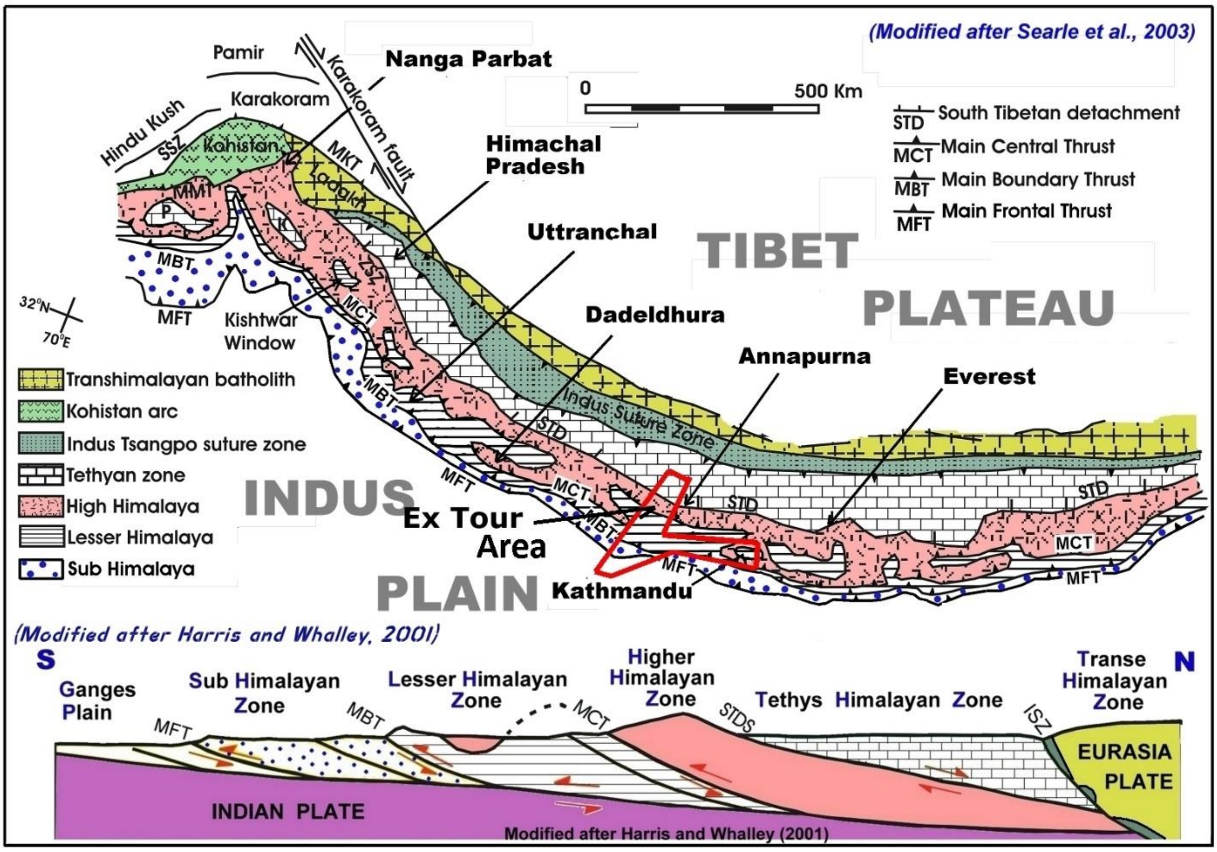

Figure 1. Geologic outline and cross section of the Himalayan Orogen with the exercise area (red frame)

The SHET-12 team included 35 Japanese and Nepali students, 3 Japanese citizens and 4 Japanese and Nepali teachers who led the team. The tour itinerary was composed of 13 days including 3 days in Kathmandu and 10 days in the field. In Kathmandu, the pre- and post field tour seminars and two days of city tour escorted by Nepali students were conducted.

The field tour of 10 days followed the route Kathmandu-Pokhara-Kaligandaki valley-Muktinath-Pokhara-Tansen-Lumbini-Narayangath-Kathmandu. An English guidebook (Yoshida and Ulak, 2017) was utilized as the exercise text throughout the field tour. The field tour used a chartered bus all through the route and hotels for all night halts. The expenses of the tour for a student was 95,733 JPY, which was reduced to 80,893 JPY by the support of 14,840 JPY per head derived from donations including the crowd funding (SHET-CF, 2024).

Reports of the tour by all participants have been assembled along with detailed logistic data of the tour in a pdf book (Yoshida, 2024) and has been presented on the book market as well as uploaded on home pages of the SHET and the Gondwana Institute for Geology and Environment (SHET-HP, 2024 and GIGE-HP, 2024).

At the presentation, some highlights of field observations in the tours including beautiful Annapurna and Dhaulagiri ranges with amazing huge and clear folding structures of the Tethys formations, a group of delighted students, and intermingling of Japanese and Nepalese students will be shown, and invitation to the 13th SHET in March 2025 will also be displayed in the presentation, along with free distribution of some useful leaflets related with the SHET program at the poster site.

Fig. 2. SHET-12 team on the Noudanda pass with the beautiful Annapurna range behind.

References

GIGE-HP, 2024, http://www.gondwanainst.org/

SHET-HP, 2024, Student Himalayan Field Exercise Project homepage. http://www.gondwanainst.org/geotours/Studentfieldex_index.htm

SHET-CF, 2024, Let us provide a chance to student to study in the Himalaya-a crowd funding. http://www.gondwanainst.org/shet-cf

Yoshida, M. and Ulak, P.D. (Eds), 2017, Geology and Natural Hazards along Kaligandaki and Highways Kathmandu-Pokhara-Butwal-Mugling. Guidebook for Student Himalayan Exercise Tour. GIGE Miscl. Pub. 35, Field Science Publishers, 144 pages.

Yoshida, M., (Ed.), 2024, Traversing the Himalayan Orogen 2024 -Report of the 12th Student Himalayan Exercise Tour in March 2024 (In Japanese and English). GIGE Miscl. Pub. 43 (e-book). Field Science Publishers, Hashimoto, Japan, 391 pages.

Yoshida, M., Arita, K., Sakai, T., Upreti B.N., 2019, Japan-Nepal joint Student Himalayan Exercise Program 7 years. Universal Journal of Geoscience, 7(1), 15-30.

Yoshida, M. and Student Himalayan Field Exercise Project, 2023, Student Himalayan Field Exercise Tour 10 years (in Japanese). Polar News 59 (1), 65-96.